

# Supernova 1987A at 10,000 Days

Richard McCray,<sup>1</sup> and Claes Fransson,<sup>2</sup>

<sup>1</sup>Department of Astronomy/University of California, Berkeley, California, USA, CA 94720-3411

<sup>2</sup> Department of Astronomy, The, Oskar Klein Centre, Stockholm University, 106 91 Stockholm, Sweden

Xxxx. Xxx. Xxx. Xxx. YYYY. AA:1–36

This article's doi:  
10.1146/((please add article doi))

Copyright © YYYY by Annual Reviews.  
All rights reserved

First page note to print below  
DOI/copyright line.

## Keywords

Supernovae, supernova remnants, nucleosynthesis, dust, molecules, shocks

## Abstract

Although it has faded since the time of the peak by a factor  $\sim 10^{-7}$ , SN1987A is still bright enough to be observed in almost every band of the electromagnetic spectrum. Today, the bolometric luminosity of the debris is dominated by a far infrared ( $\sim 200 \mu\text{m}$ ) continuum from a massive ( $\sim 0.5 M_{\odot}$ ) reservoir of dust grains in the interior debris. The dust absorbs and is heated by UV, optical, and near-infrared emission resulting from radioactive energy deposition by  $^{44}\text{Ti}$ .

The optical light of the supernova debris is now dominated by illumination of the debris by thermalized X-rays resulting from the impact of the outer supernova envelope with an equatorial ring of gas that was expelled some 20,000 years before the supernova explosion. X-ray and optical observations trace a complex system of shocks resulting from this impact, while radio observations trace synchrotron radiation from relativistic electrons accelerated by these shocks. The luminosity of the remnant is dominated by near-infrared ( $\sim 20 \mu\text{m}$ ) continuum from dust grains in the equatorial ring heated by collisions with ions in the X-ray emitting gas.

With the Atacama Large Millimeter Array (ALMA) we can observe the interior debris at mm/sub-mm wavelengths, which, unlike optical and near-infrared wavelengths, are not absorbed by the interior dust. The early ALMA observations reveal bright emission lines from rotational transitions of CO and SiO lines that provide a new window into the interior structure of the supernova debris.

Intensive searches using instruments at every band of the electromagnetic spectrum have failed to yield any evidence for the compact object expected to reside at the center of the remnant. The current upper limit to the luminosity of such an object is a few tens of solar luminosities.

## Contents

1. INTRODUCTION .....	2
2. ENERGY SOURCES AND LIGHT CURVES .....	4
3. THE DEBRIS.....	9
3.1. Optical/IR emission .....	9
3.2. Ejecta structure .....	10
3.3. Dust formation .....	13
4. CIRCUMSTELLAR MATTER .....	14
4.1. The impact .....	17
4.2. The Reverse Shock.....	20
4.3. X-ray Emission .....	22
4.4. Dust emission from the ring .....	25
4.5. Radio emission .....	26
4.6. VHE gamma-rays .....	27
5. HOW UNIQUE WAS SN 1987A?.....	28
6. THE FUTURE.....	30

## 1. INTRODUCTION

This is the third review of SN1987A in this series. In the first, Arnett et al. (1989) reviewed the observations made during the first two years after the discovery of the event. Observations of the initial burst of neutrinos were consistent with the notion that the core of the progenitor collapsed and formed a compact object, most likely a neutron star. The optical light curve resulted from diffusion of radiation produced by the decay sequence  $^{56}\text{Ni} \rightarrow ^{56}\text{Co} \rightarrow ^{56}\text{Fe}$  through the expanding envelope of a massive blue supergiant progenitor (mass estimated to be 16-22  $M_{\odot}$  initially and  $\sim 14 M_{\odot}$  at the time of explosion). They described the early emergence of gamma rays from the decay of  $^{56}\text{Co}$  and of hard X-rays resulting from the Compton scattering of the gamma rays. The observations of narrow UV emission lines first seen with the IUE satellite indicated the presence of circumstellar matter near (within  $\sim 1$  lt-yr) the supernova, evidently expelled by the supernova progenitor.

In the second review, McCray (1993) revisited the evidence that the light curve of SN1987A was powered by radioactivity and described how it would be dominated at late times by longer-lived isotopes such as  $^{57}\text{Co}$  and  $^{44}\text{Ti}$ . By  $\sim 4$  months the supernova debris became optically thin in the optical/infrared continuum and its spectrum was dominated by emission lines. Analysis of the nebular spectrum showed that fragments of different elemental composition in the debris had different temperature evolution. By  $\sim 200$  days vibration bands of CO and SiO appeared in the infrared spectrum, indicating temperatures  $T \lesssim 4000$  K, which decreased to  $T \lesssim 2000$  K by  $\sim 400$  days. In the interval 400 – 500 days dust formed in the debris, rendering most of the inner debris obscure to optical and near-IR radiation and converting most of this radiation to far-infrared continuum. Images obtained with the ESO NTT telescope and the Hubble Space Telescope showed that the nebulosity emitting the narrow UV lines was coming from a system of three circumstellar rings, leading to predictions that the supernova blast wave would strike the ring within several years.

In the 22 years that have elapsed since the second review was published, we have learned much about the supernova and its evolution, thanks largely to powerful new facilities that

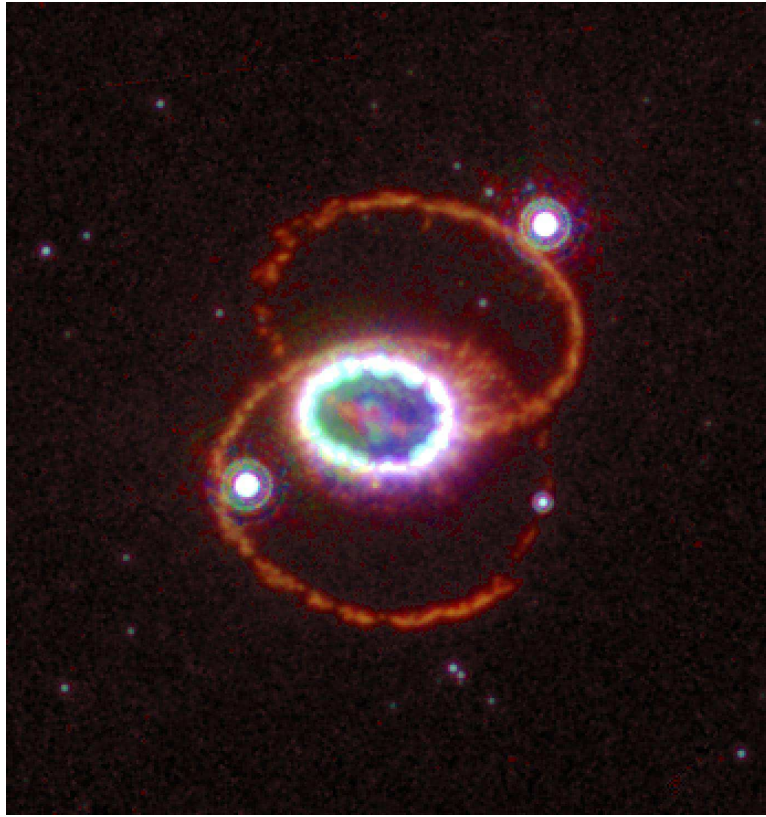


**Figure 1**

Composite image of SN1987A in H $\alpha$  with the Hubble Space Telescope. Images from three epochs have been stretched and combined to enhance different components. Red – as seen by WFPC2 in 1994-1997; Blue – as seen by ACS in 2001-2004; Green – as seen by WFPC3 in 2009-2014.

Courtesy of Peter Challis

have become available in the interval. Despite the fact that its bolometric luminosity has faded by a factor  $\sim 10^{-7}$ , SN1987A is still bright enough to be observed in almost every band of the electromagnetic spectrum. The repaired Hubble Space Telescope has produced images of the debris and triple ring system (**Figure 1**), while telescopes empowered with adaptive optics such as the VLT and Gemini have yielded images and spectra far superior to those previously available. The Chandra and XMM observatories have tracked the evolution of the image and spectrum of the X-ray emitting gas. The INTEGRAL and NUSTAR observatories have enabled us to observe the predicted gamma rays from the decay of  $^{44}\text{Ti}$ . The Spitzer Observatory has yielded spectra in the mid-IR, while the Herschel Observatory gave us the first opportunity to see the supernova at far-IR wavelengths since 1995, when the Kuiper Airborne Observatory ceased operations. The Australia Compact Telescope Array (ATCA) has tracked the evolution of the image of non-thermal radio emission in the cm and mm bands. Most recently, the Atacama Large Millimeter Array (ALMA) has enabled us for the first time to resolve the inner supernova debris at mm/sub-mm wavelengths, free of the obscuration by dust that limits our view in the optical and near-IR bands.

Meanwhile, the supernova itself has evolved dramatically. Some aspects have proceeded according to script. The predicted impact of the supernova debris with its circumstellar equatorial ring (ER) is now fully underway, so that the bolometric luminosity is now dominated by X-ray and mid-IR emission from the shocked gas and dust in the ring. The luminosity of the inner debris is dominated by the decay of  $^{44}\text{Ti}$ . But other aspects have been surprising. 'Hotspots' in the HST images showed that the ring contained clumps of gas having density an order of magnitude greater than the average. The Herschel observatory revealed that a substantial fraction of the nucleosynthesis products resides in a massive reservoir of dust in the inner debris, while the ALMA observatory has yielded evidence of the presence of CO and SiO molecules having net mass comparable to the dust mass.

Despite all this progress, mysteries remain. Large departures from spherical or even cylindrical symmetry in both the supernova debris and the circumstellar matter still lack satisfactory explanations. Except for the neutrino pulse, no evidence has yet appeared for the compact object that must have formed in the core collapse.

In the following, we review this progress and the outstanding issues, concluding with some speculations about future progress that we may expect in future studies of this fascinating and unique phenomenon.

## 2. ENERGY SOURCES AND LIGHT CURVES

**Figure 2** shows the light curves of SN1987A and its components. The bolometric light curve was dominated by optical light (the cyan curve) for the first 500 days. By 120 days, the photosphere had vanished and the light had a 'nebular' spectrum, dominated by emission lines, as described by McCray (1993). This optical light tracked the exponential decay ( $t_{56} = 111.3$  d) of radioactive energy deposited in the debris until about 500 days, corresponding to a  $^{56}\text{Ni}$  mass of  $0.069 \pm 0.003 M_{\odot}$ .

At  $t \sim 500$  days, a dramatic change occurred in the light curve and spectrum. The optical light rapidly dropped below the  $^{56}\text{Co}$  decay luminosity. At the same time, a far-IR continuum appeared (Wooden et al. 1993, and references thereon). The combined luminosities of the optical light, the far-IR continuum, and escaping gamma rays continued to track the exponential decay of  $^{56}\text{Co}$ . Evidently, this change was due to the formation of dust grains within the debris, which absorbed the optical and near-IR radiation. The dust grains had temperature  $T_d \sim 600$  K (McCray 1993). The red sides of the optical and near-IR emission lines nearly vanished, indicating that the dust was almost completely blocking the optical/near-IR emission from the far side of the debris.

At roughly the same time, vibration-rotation bands of CO and SiO appeared. Analysis of these bands (Liu, Dalgarno & Lepp 1992) indicated that these molecules had masses  $M_{CO} \approx 10^{-3} M_{\odot}$  and  $M_{SiO} \approx 10^{-3} M_{\odot}$ , respectively. When first detected, at  $t = 192$  days, the CO had temperature  $T_{CO} \approx 4000$  K, which dropped to  $T_{CO} \approx 1800$  K at  $t = 377$  days.

Pinto, Woosley & Ensman (1988), Woosley, Hartmann & Pinto (1989) and Hashimoto, Nomoto & Shigeyama (1989) predicted that, by  $t \approx 1200$  days, the energy deposition in the supernova debris would be dominated by the decay of the longer-lived ( $t_{57} = 390d$ ) isotope  $^{57}\text{Co}$ . In addition, as Fransson & Kozma (1993) pointed out, recombination of residual HII ions could make a contribution to the light curve comparable to that from  $^{57}\text{Co}$ . They could account for the observed bolometric light curve for  $t > 1000$  days with  $M_{57} \approx 0.003 M_{\odot}$  of  $^{57}\text{Co}$ , close to the value  $M_{57} \approx 0.002 M_{\odot}$  predicted by Woosley et al. and Hashimoto et al.

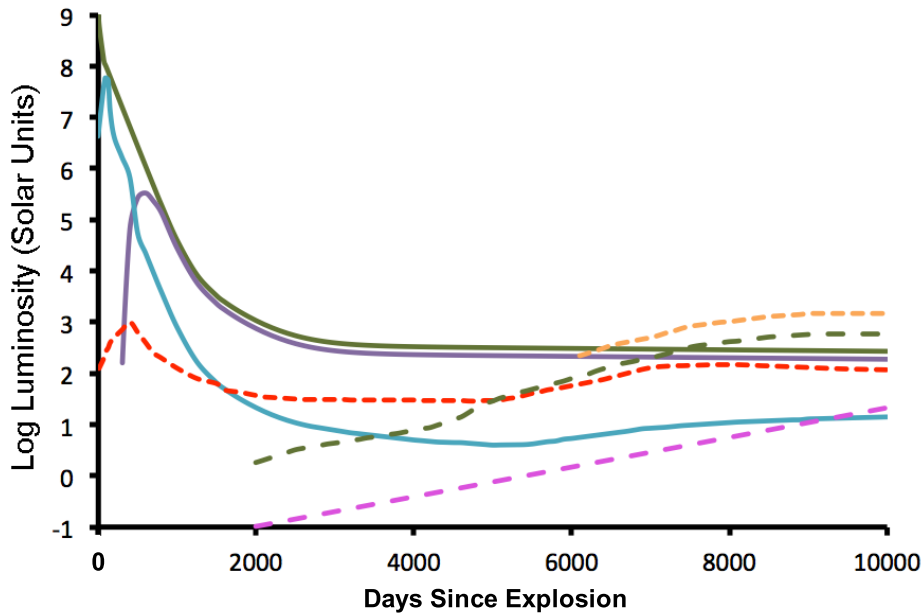


**Figure 2**

SN1987A Light Curves. Solid curves are debris: Green – Radioactive deposition (Fransson & Kozma 2002; Jerkstrand, Fransson & Kozma 2011; Boggs et al. 2015); Violet – Far-Infrared (McCray 1993; Matsuura et al. 2015); Cyan – Optical (McCray 1993; Larsson et al. 2011; Jerkstrand, Fransson & Kozma 2011, J. Larsson, priv. comm.). Dashed curves are equatorial ring: Pink – Radio (3–20 cm) (Manchester et al. 2002; Zanardo et al. 2010, 2014; Ng et al. 2013); Green – X-rays (0.5 – 3 keV) (Hasinger, Aschenbach & Truemper 1996; Burrows et al. 2000, Frank et al. 2015, *in prep.*); Red – UV/Optical (Lundqvist & Fransson 1991; Mattila et al. 2010; Fransson et al. 2015); Gold – Near Infrared (5 – 30  $\mu\text{m}$ ) (Dwek et al. 2008, 2010).

These authors also predicted that the luminosity of SN1987A would be dominated for  $t > 7$  years by the decay of  $^{44}\text{Ti}$  ( $t_{44} = 85$  years). The radioactive energy is deposited in the debris by stopping of fast (596 keV) positrons from the prompt decay of  $^{44}\text{Sc}$ , the daughter of  $^{44}\text{Ti}$  (e.g., Seitzzahl, Taubenberger & Sim 2009). The estimated  $^{44}\text{Ti}$  mass was  $M_{44} \approx 10^{-4} M_{\odot}$ . Their prediction was confirmed with the detection by the INTEGRAL (Grebenev et al. 2012) and NUSTAR observatories (Boggs et al. 2015) of 67.9 keV and 78.4 keV gamma ray lines emitted as a result of the decay of  $^{44}\text{Ti}$  (**Figure 3**). The mass of  $^{44}\text{Ti}$  inferred from the NUSTAR observation was  $M_{44} = (1.5 \pm 0.3) \times 10^{-4} M_{\odot}$ , significantly less than the value  $M_{44} = (3.1 \pm 0.8) \times 10^{-4} M_{\odot}$ , inferred from the earlier INTEGRAL observation.

In what form does this energy emerge? In a detailed model for energy deposition and spectrum formation, Jerkstrand, Fransson & Kozma (2011) estimate a mass  $M_{44} = (1.5 \pm 0.5) \times 10^{-4} M_{\odot}$ , consistent with the NUSTAR observation. **Figure 4** shows a model fit to the spectrum at  $\sim 8$  years together with HST observations from Chugai et al. (1997). This  $^{44}\text{Ti}$  mass also agrees with a nebular analysis of the Fe II emission lines based on the same spectrum by Chugai et al. The spectrum at this epoch is radically different from the thermally dominated spectrum during the first  $\sim 500$  days, discussed in McCray (1993). In

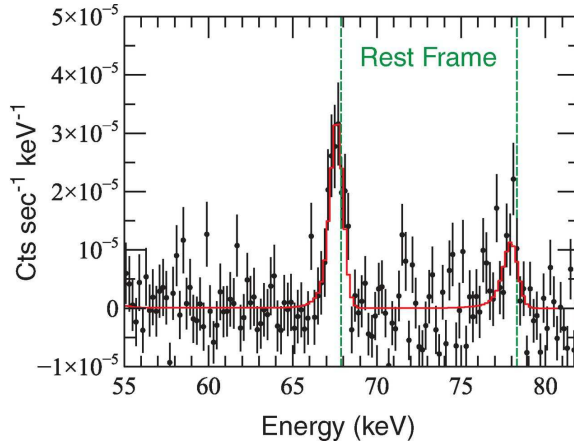


**Figure 3**

Gamma-ray spectrum of SN 1987A from NUSTAR (Boggs et al. 2015)

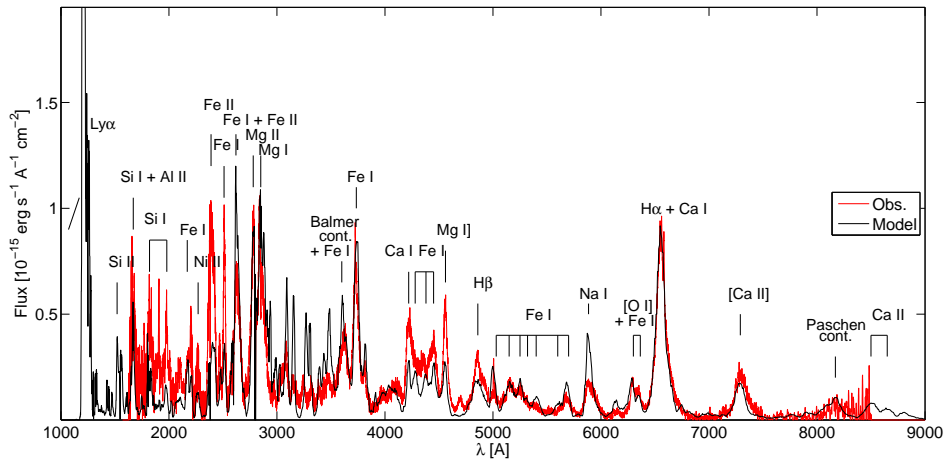


**Figure 4**

Optical/UV spectrum of SN 1987A at  $\sim 8$  years from HST (red) (Chugai et al. 1997) together with model spectrum (black) (from Jerkstrand, priv. comm., as calculated in Jerkstrand, Fransson & Kozma 2011). Note the strong UV emission and the low state of ionization. The optical/UV spectrum at this epoch is dominated by non-thermal excitation and ionization. The  $^{44}\text{Ti}$  mass was  $1.5 \times 10^{-4} M_{\odot}$ .

the  $^{44}\text{Ti}$  dominated phase the temperature is  $\lesssim 200$  K and the only lines which are excited thermally are fine structure lines in the mid-IR and rotational lines from molecules. All lines in the UV and optical are a result of non-thermal excitation by the fast electrons, resulting from the positrons from the  $^{44}\text{Ti}$  decay. The gamma-rays from the  $^{44}\text{Ti}$  decay escape freely at this epoch and the total energy input from the positrons at 10,000 days is  $\sim 278 L_{\odot}$ .

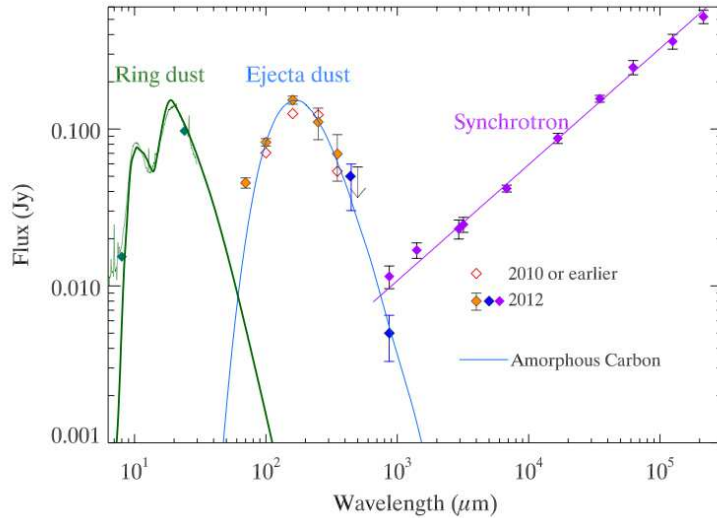


**Figure 5**

SN 1987A Spectral Energy Distribution Matsuura et al. (2015). Green – data from Spitzer observatory and fit to silicate emission from ER. Orange – data from Herschel observatory. Blue – data from ALMA. Violet – data from ATCA and MOST.

Because of the low  $^{44}\text{Ti}$  input the plasma is nearly neutral, as is seen from the strong Fe I lines in the spectrum (Fig. 4). With an electron fraction of  $\sim 0.2$  approximately 60% of the positron input goes to heating of the thermal electrons (Kozma & Fransson 1992), while the rest goes to ionization and excitation of UV and optical lines. Jerkstrand et al. find that most of the heating should be emitted in the [FeII]  $26\ \mu\text{m}$  line, resulting in a  $26\ \mu\text{m}$  luminosity of  $\sim 0.6 \times 278 L_{\odot} = 167 L_{\odot}$ . This is, however, more than an order of magnitude greater than observed (Bouchet et al. 2006).

In an observation with the Herschel observatory, Matsuura et al. (2011) discovered a luminous ( $\sim 220 L_{\odot}$ ) source of far-infrared ( $100 - 500\ \mu\text{m}$ ) continuum at the location of SN1987A (**Figure 5**). Lakićević et al. (2012b) confirmed this finding in observations at  $350$  and  $870\ \mu\text{m}$  with the Atacama Pathfinder Experiment (APEX). In subsequent observations with the ALMA observatory, Indebetouw et al. (2014) found that the infrared source was coincident with the expanding debris. This continuum is evidently produced by dust grains in the debris. A fit to the spectrum showed that the grains have temperature  $T_d = 17 - 23$  K. Matsuura et al. (2015) were able to fit the spectrum observed by HERSCHEL and ALMA, with a model consisting of  $0.5 \pm 0.2 M_{\odot}$  of amorphous carbon or a mix of  $0.3 M_{\odot}$  of amorphous carbon and  $0.3 M_{\odot}$  of silicates, e.g.,  $\text{MgSiO}_3$ . More recently, Dwek & Arendt (2015) found that elongated composite grains consisting of  $\sim 0.4 M_{\odot}$  of silicates and  $\sim 0.05 M_{\odot}$  of amorphous carbon could account for the far-infrared spectrum. In any case, the result is astonishing, as it requires almost all of the magnesium and silicon expected from nucleosynthesis models to have condensed into grains.

Such a large mass in grains is sufficient to absorb most of the optical and near-IR luminosity produced by radioactive energy deposition in the debris. Depending on its composition and distribution in the debris, the dust may have sufficient optical depth to

absorb most of the [FeII] 26 $\mu$ m line as well. If so, the far-IR continuum observed with Herschel is a bolometer of the radioactive energy deposition rate.

The Fe I dominated spectrum in Fig. 4, as well as the centrally peaked 1.644 $\mu$ m Si I/Fe II emission with SINFONI/VLT (Kjær et al. 2010; Larsson et al. 2013), show that the observed optical/NIR spectrum from the core is dominated by reprocessed radiation from the  $^{44}\text{Ti}$  radioactivity. Jerkstrand, Fransson & Kozma (2011) estimate that of the  $\sim 40\%$  of the  $^{44}\text{Ti}$  input going into UVONIR emission  $\sim 65\%$  is absorbed by the dust, or  $\sim 0.4 \times 0.65 \times 278 L_{\odot} = 72 L_{\odot}$ . The remaining  $\sim 60\%$  goes to heating, which is mainly balanced by emission in the Fe II 26  $\mu$ m line. The escaping UVONIR luminosity is therefore only  $\sim 14\%$  of the total.

Adding up the dust absorbed energy one finds a luminosity of  $167 + 72 = 239 L_{\odot}$ , which is within the errors of that derived from the Herschel/ALMA dust emission. One therefore finds a consistent energy budget for the ejecta at these late epochs.

As discussed above, we require the dust to absorb nearly all radiation in the 10–100  $\mu$ m band. At the same time it must not absorb all the optical/NIR radiation. One possibility is absorption by optically thick silicates, such as  $\text{MgSiO}_3$  and  $\text{MgSiO}_4$ , which have an opacity in the 10-30  $\mu$ m range a factor  $\sim 10^2 - 10^3$  greater than that at optical wavelengths (Jäger et al. 2003). Corundum ( $\text{Al}_2\text{O}_3$ ) has a similar optical properties. However, there is evidence for a nearly constant dust absorption in the optical band from  $\sim 500$  to 10,000 days. Possibly, this is due to a second component of optically thick carbon dust with a covering factor  $\sim 0.65$ . Silicates, corundum and carbon dust are the most abundant grains found in simulations of clumpy ejecta by Sarangi & Cherchneff (2015).

A new phase in the energy budget commenced at about day 5000. Up to this epoch the luminosity of the ejecta had decreased slowly due to the  $^{44}\text{Ti}$  decay. Photometry in the R and B bands with HST, however, showed that after this epoch the luminosity increased steadily by a factor of 3–4 at 10,000 days (Larsson et al. 2011, and J. Larsson priv. comm.). Evidently, X-rays from the ring interaction (Sect. 4.3) absorbed and thermalized by the ejecta now contribute more to the optical luminosity than the  $^{44}\text{Ti}$  decay. Adding up the radioactive contribution and a fraction of  $\sim 5\%$  of the X-ray luminosity yields a qualitative agreement with the optical light curves.

This change may be regarded as marking a transition to the remnant phase, when the luminosity is dominated by interaction rather than radioactive input. At the same time the optical morphology changed from centrally dominated emission to a horse-shoe like shape (Fig. 1). (Fransson et al. 2013). One finds that X-rays with energy of 2 keV can penetrate into the metal core of the ejecta. At this point the photoelectric absorption by the metals becomes large enough to shield most of the core from the X-rays. It is therefore mainly the hydrogen and helium envelope which is affected by the X-rays. This accounts for the change of morphology of the ejecta in the X-ray dominated phase.

Because of the greater photoelectric cross section, approximately  $\sigma \propto E^{-3}$ , X-rays with energy  $\lesssim 1$  keV are mainly absorbed in the outer parts of the ejecta, close to the reverse shock, which may explain the  $\text{Ly}\alpha$  emission from this region (France et al. 2015). The X-rays have a similar effect as the positrons and gamma rays. The secondary electrons resulting from the photoelectric absorption will lead to excitation, ionization and heating of the envelope, which result in  $\text{Ly}\alpha$ ,  $\text{H}\alpha$  and IR emission from especially the high velocity hydrogen envelope (Xu & McCray 1991; Kozma & Fransson 1992).



### 3. THE DEBRIS

Typical models of a core-collapse supernova progenitor have a laminar structure, with nested layers of Si/S, O/Ne, C/O, He, and H surrounding a core of Fe. Instabilities before and after the explosion will cause this structure to fragment into 'clumps' of different elemental composition that are no longer radially segregated. This mixing is macroscopic, not microscopic, as evidenced by the fact that the temperatures inferred from line ratios of different species are not the same. (McCray 1993).

#### 3.1. Optical/IR emission

During the last decade there has been considerable progress in modeling the early spectra and light curve. In particular, Utrobin & Chugai (2005) have shown that time dependent effects are important for the ionization of the outer hydrogen envelope. This results in a higher envelope ionization than in steady state, and is important in order to get a proper strength of the H $\alpha$  line, without invoking clumping or radioactive excitation. This freeze-out of the ionization is analogous to that occurring at very late stages for the inner parts of the ejecta (Fransson & Kozma 1993). Utrobin & Chugai (2005) further show that the overabundance of barium, claimed earlier, can also be explained as a result of the higher ionization in the time dependent models. The importance of a time dependent treatment has been confirmed by Dessart & Hillier (2010) in more detailed models, who also find that there is no need for any extra radioactive source at high velocity to explain the strength of the HI and HeI lines, as has been discussed in early papers. These models probably represent the best reproduction of the spectra and light curve during the first month after explosion, albeit in the context of 1-d models.

The formation and diagnostics of the different optical and IR lines in the nebular phase were reviewed in McCray (1993). Fully self-consistent models of the thermal evolution of the different composition zones up to 2000 days have been calculated by Kozma & Fransson (1998b,a) and de Kool, Li & McCray (1998). An important result of these calculations is that the temperature of the different composition zones differ substantially, depending on the energy input, densities and compositions. The Fe dominated zones drop below 1000 K at  $\sim 500$  days, and the Si and O rich zones somewhat later. The temperature evolves more slowly in the H and He zones, where adiabatic cooling becomes important after 600 days, and only reaches 1000 K by day 1200. In the metal-rich zones IR fine-structure lines cause a thermal instability to  $\lesssim 200$  K in only  $\sim 200$  days. This is reminiscent of the 'IR-catastrophe' discussed for Type Ia supernovae (Axelrod 1980).

Between  $\sim 800 - 1500$  days the Fe I-II emission is dominated by primordial iron, rather than the synthesized iron, which dominates before and also after this period. The same is true for the [Ca II]  $\lambda 7300$  lines, the emission of which is dominated by the O and H rich zones, not by the Si/S zone where most of the newly synthesized Ca resides (Li & McCray 1993; Kozma & Fransson 1998a). This is an important lesson for the analysis of other core collapse supernovae. Later than  $\sim 1500$  days, when positrons from  $^{44}\text{Ti}$  dominates the energy input, almost all emission is from the Fe rich zones, except the H and He emission from the slowly recombining envelope.

Although the ejecta in the nebular phase is optically thin in the continua of the excited levels of H and He, it may still have a significant opacity in the many optically thick resonance lines, especially of the Fe group elements (Li & McCray 1996). Even at 8 years there was significant blocking of the UV emission, resulting in a transfer of the UV emission

into the optical by multiple scattering and fluorescence (Jerkstrand, Fransson & Kozma 2011).

The models above did not include molecular formation and cooling. In particular, vibrational cooling by CO and SiO can be important in the zones where C/O and O/Si respectively are abundant. This was demonstrated for CO by Liu & Dalgarno (1995), who find that in the zone where C is abundant together with O cooling is dominated by CO. The emission in the fundamental band at  $4.6 \mu\text{m}$  follows the gamma-ray input to the C/O zone, in agreement with observations. This argues against microscopic mixing of He into this zone, where any  $\text{He}^+$  would destroy the CO.

## 3.2. Ejecta structure

During the past few decades, substantial progress has been made in understanding the mechanism for core-collapse supernovae. Several independent groups have demonstrated that neutrino-driven convection will drive large scale instabilities leading to a supernova explosion (e.g., Janka et al. 2012). But major uncertainties remain, particularly with respect to the roles of rapid rotation and magnetic fields. Observations of the distribution and kinematics of nucleosynthesis products in the ejecta of SN1987A offer the possibility of testing and discriminating among theoretical models for the explosion. As we describe in the following, our knowledge of structure of the ejecta is still fragmentary; but it is advancing rapidly thanks to new instrumental facilities at several wavelengths.

**3.2.1. Observations.** Evidence for large-scale asymmetry in the ejecta emerged within a few months of the explosion. Fine structure appeared in the profile of  $\text{H}\alpha$  (the 'Bochum event' (Hanuschik & Thimm 1990)) indicating inhomogeneities in the emission by hydrogen expanding with velocities  $\sim 4500 \text{ km s}^{-1}$ . The appearance of X-rays and gamma rays earlier than predicted indicated that some of the newly synthesized  $^{56}\text{Co}$  had penetrated into the hydrogen outer layer of the ejecta (McCray 1993).

Wang et al. (2002) have suggested these observations, along with observations of asymmetry inferred from speckle interferometry (Papaliolios et al. 1989) and spectropolarimetry, could be explained if the supernova explosion was driven by jets aligned with the major axis of the debris. But it is also possible that these phenomena can be explained without invoking the jet hypothesis.

A unique set of information about the asymmetry at the early epochs, close to maximum light, comes from spectroscopic observations of dust light echoes around SN 1987A (Sinnott et al. 2013). In particular, fine structure in the  $\text{H}\alpha$  line, similar to the Bochum event, was seen to vary with the position angle on the light echo rings, indicating an asymmetry in the hydrogen envelope. The direction of the asymmetry agrees well with that inferred from the VLT observations, which, however, refer to the inner metal core.

From images reconstructed through speckle interferometry, Nisenson et al. (1987) reported the detection of a source of optical emission displaced from the supernova center by  $0.06''$ . This so-called 'Mystery Spot' was very bright – only 2.7 magnitudes fainter than the supernova at  $t = 1$  month. We are unaware of any plausible physical explanation for this phenomenon. If the Mystery Spot is real, we find it difficult to understand how it could fail to leave any spectroscopic trace of its existence.

Most of the hydrodynamics of the explosion plays out within several hours, except for the expansion of the 'nickel bubbles' (Woosley 1988; Herant & Benz 1991; Li, McCray

& Sunyaev 1993), driven by deposition of radioactive energy by  $^{56}\text{Ni}$ , which has a mean lifetime of 8.8 days. After a time  $\Delta t \sim$  few weeks, all acceleration had ceased, the debris was coasting, and the structure was expanding homologously. Accordingly, gas in the debris emitting spectral lines having Doppler shift,  $V_D$ , is confined to a thin sheet displaced a distance  $z \approx V_D t$  along the line of sight from the center of the explosion, where  $t$  is the time since explosion. The sheets of constant Doppler shift are very nearly planar, departing from flatness by  $\Delta t/t \sim 10^{-3}$ .

Today, the supernova debris is quite cold. For example, a fit to the observations of rotational emission lines of CO by Kamenetzky et al. (2013) implies that  $T(\text{CO})$  is probably  $< 100$  K. It follows that the mean molecular velocity of the emitting gas,  $c_S \sim (kT/\mu)^{1/2} < 0.2 \text{ km s}^{-1}$ , is far less than the typical expansion velocity of the debris, the emission lines of which have  $\text{FWHM} \approx 3000 \text{ km s}^{-1}$ . Thus, the fractional thickness of a sheet emitting at a given Doppler shift is  $\sim c_S/V_D \sim 10^{-4}$ .

The fact that the Doppler shift maps directly to depth enables one to infer the structure of the debris in three dimensions from observations of images within emission lines. A dramatic example of this technique was provided by Kjær et al. (2010) and Larsson et al. (2013), who mapped the debris with the integral field spectrograph SINFONI on the VLT. As Figure 1 shows, the optical image of the debris at late times is an irregular homunculus elongated in the N/S direction. Most people had assumed that this elongation implied that the debris was prolate, with the N/S extension in the polar direction. If so, the northern lobe of the debris would be red-shifted and the southern lobe, blue-shifted. But the observations contradicted this picture: the northern lobe was blue-shifted and the southern lobe was red-shifted. These results show that the debris is triaxial, with the northern extension in the plane of the equatorial ring and the southern extension in the plane of the sky. The quest to map the debris in three dimensions is confounded by the internal dust, which is certainly obscuring our view of much of the far hemisphere, as evidenced by the fact that the red wings of the emission lines that vanished when the dust began to form have not reappeared.

In fact, the optical emission from the debris of SN1987A is now driven primarily by X-rays shining into the debris (Larsson et al. 2011) from shocked gas near the equatorial ring. This explanation accounts for the facts that the optical image of the debris has become brighter and appears to be concentrated in the equatorial plane. The dark spot near the center of the optical image (Figure 1) could be due to the fact that the soft X-rays do not penetrate to the center and/or due to a dust cloud in the near hemisphere.

With the commissioning of the Atacama Large Millimeter Array (ALMA), we have a new window on the inner debris. Unlike optical or near-IR radiation, mm/sub-mm radiation is not absorbed by dust grains. Kamenetzky et al. (2013) observed SN1987A in early science observations with a partial (14 – 18 dishes) array in compact (400 m maximum baseline) configuration and found surprisingly strong emission lines from rotational transitions of CO (1-0 and 2-1) and SiO (5-4) (**Figure 6**). They find that the CO has a minimum mass  $M_{\text{CO}} > 0.01 M_{\odot}$  and temperature  $T_{\text{CO}} = 10 - 100$  K. This mass is at least an order of magnitude larger than that inferred from the vibrational lines during the first years,  $\sim 10^{-3} M_{\odot}$  (Liu, Dalgarno & Lepp 1992).

Even without resolving the debris, early observations with ALMA (Matsuura et al. 2015) have already given us evidence that the spatial distribution of SiO differs from that of CO. The line profiles are different. Moreover, the SiO line profiles have a 'dip' at their centers – clear evidence for departure from spherical symmetry in the distribution of SiO.

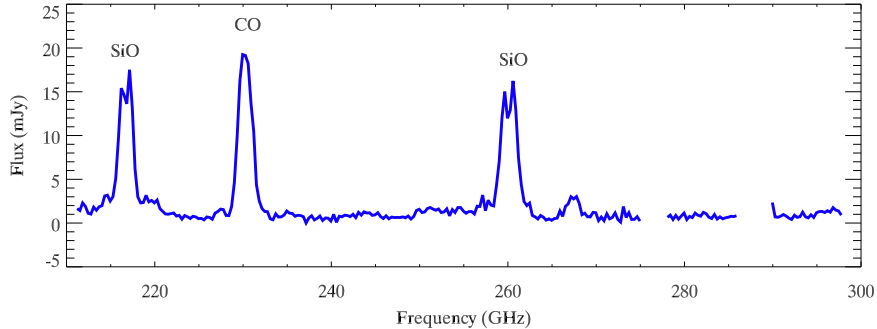


**Figure 6**

ALMA spectrum of SN1987A, showing bright emission lines of CO( $J = 2-1$ ) and SiO( $J = 5-4$  and  $J = 6-5$ ) from the inner supernova debris (Matsuura et al. 2015, in preparation). Note central dip in the SiO line profiles, which is not present in the CO profile.

The ALMA early science observations had angular resolution  $\sim 1''$ , sufficient to demonstrate that the CO emission originates in the inner debris of SN1987A but not sufficient to resolve the debris. But when the array is operating at its maximum baseline, it will be able to resolve the CO ( $2-1$ ) emission with angular resolution  $\sim 0.04''$ , comparable to the Hubble Space Telescope. With that resolution, the ALMA should be able to see the kind of structure in the debris predicted in 3-d hydrodynamic simulations.

**3.2.2. Hydrodynamical models.** Theoretical models incorporating increasingly realistic physics both for the hydrodynamics and neutrino transport are being developed by several groups (see Janka 2012; Janka et al. 2012; Burrows 2013, for reviews). Much work remains, however, until one can say for sure that the explosion mechanism is understood. In particular, the interplay between convective motions and nuclear burning during the last burning phases of the progenitor may change substantially the outcome of the explosion (e.g., Herant, Benz & Colgate 1992; Herant et al. 1994; Couch et al. 2015, and references therein).

The observational probes of the explosion mechanism include the neutrino burst, masses and distribution of the radioactive nuclei,  $^{56}\text{Ni}$ ,  $^{57}\text{Ni}$  and  $^{44}\text{Ti}$ , other abundant elements, like C, O and Si, the morphology of the ejecta, and pulsar kick velocities and spins. Pulsar properties and nucleosynthesis yields are sensitive to the explosion mechanism. An important clue is the recent observation by Boggs et al. (2015) that the 68 and 78 keV emission lines from  $^{44}\text{Ti}$  decay are red-shifted by  $700 \pm 400 \text{ km s}^{-1}$  relative to the supernova rest frame.

There has been some progress in relating the structure and dynamics during the first second to morphology and kinematics that can be observed after the shock break-out. In particular, Hammer, Janka & Müller (2010), and Wongwathanarat, Müller & Janka (2015) have made 3-d calculations from the core collapse up to the shock breakout. The authors of

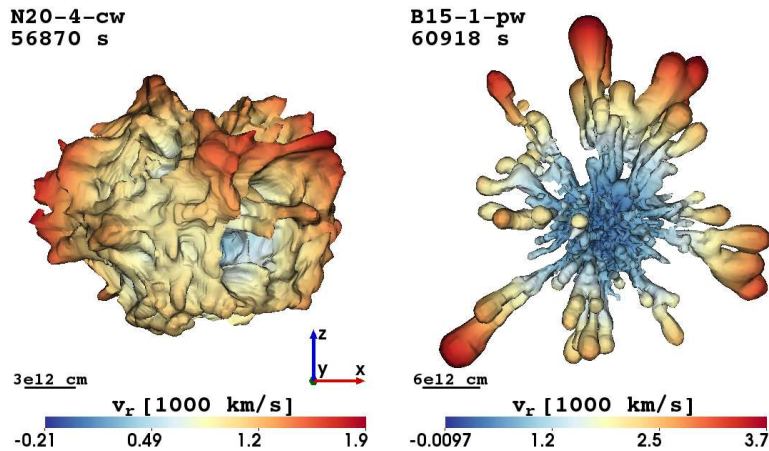


**Figure 7**

Isocontours of the  $^{56}\text{Ni}$  distribution for a  $20 M_{\odot}$  (left) and  $15 M_{\odot}$  (right) progenitor  $\sim 16$  hours after explosion (Wongwathanarat, Müller & Janka 2015). The color bars give the expansion velocity of the surface. Note the higher velocities in the strongly fragmented distribution for the  $15 M_{\odot}$  model. The heating from the  $^{56}\text{Ni}$  decay has not been included.

the latter paper find that the initial structure is significantly affected by the reverse shock and by the asymmetries resulting from the neutrino heating (**Figure 7**).

These authors also find that the structure is sensitive to whether the progenitor is a compact blue supergiant, like that of SN 1987A, or a red supergiant. In the former case they also find significant differences between a  $15 M_{\odot}$  and a  $20 M_{\odot}$  progenitor, which is probably related to the different density gradients in the inner core. Their models are only calculated up to less than a day and do not include the heating from the  $^{56}\text{Ni}$  decay, which may change the hydrodynamic structure appreciably (Herant & Benz 1991; Li, McCray & Sunyaev 1993).

Mapping these 3-d models into 1-d, Utrobin et al. (2014) have simulated light curves of SN 1987A. They find a good agreement of the main diffusion peak at  $\sim 100$  days with a  $15 M_{\odot}$  model. Their results are a major improvement compared to the earlier, artificially mixed models designed to reproduce the light curve. However, their models do not reproduce the early cooling phase during the first days and the general evolution during the first  $\sim 40$  days. Another problem is that the core mass of their  $15 M_{\odot}$  model is too low to explain the progenitor, while the  $20 M_{\odot}$  model, which has the necessary core mass, has too little mixing. The authors suggest a more compact progenitor, possibly indicating a binary origin.

### 3.3. Dust formation

There are conflicting scenarios for the dust formation in SN 1987A. Wesson et al. (2015) model the NIR to FIR SEDs at various epochs for different assumptions about the grain composition and sizes. They find that only  $\sim 0.003 M_{\odot}$  of dust could have formed at 1152 days, the last epoch at which FIR spectra were obtained before 8467 days, when Herschel observations became available. According to their models, the grains are dominated by carbon with only  $\sim 15\%$  of silicates. At the Herschel epochs the grains must be large,

$> 3 \mu\text{m}$ , while at the earlier epochs the grains must be at least an order of magnitude smaller. They concluded that most of the grain growth had to take place later than  $\sim 3$  years and mainly by coagulation.

In contrast, Sarangi & Cherchneff (2015) find, from detailed kinetic modeling of the dust nucleation and condensation, that most of the grain mass must be formed before  $\sim 1200$  days. For a model including realistic clumping this event occurred even earlier, at  $\sim 500$  days. Further, they find that the epoch of formation differed greatly for different species and that the size distribution was very different from that of a standard MRN distribution, as Wesson et al. (2015) assumed.

According to Sarangi & Cherchneff (2015), most of the dust was in silicates with a smaller fraction of carbon, but also included pure Mg, Si and Fe grains. Also the grain sizes and total dust mass were found to be sensitive to clumping. For their clumpy model they found a total dust mass of  $\sim 0.13 M_{\odot}$ , while a more uniform distribution only gave  $\sim 0.03 M_{\odot}$  at the final epoch.

More recently, (Dwek & Arendt 2015) proposed a model in which  $\sim 0.4 M_{\odot}$  of dust formed at early times,  $t \lesssim 500$  days. The grains have ellipsoidal shapes and are composed primarily of silicates with amorphous carbon inclusions. The net masses of refractory elements,  $\sim 0.09 M_{\odot}$  of Mg,  $\sim 0.1 M_{\odot}$  of Si, and  $\sim 0.046 M_{\odot}$  of C in the grains do not violate expected nucleosynthesis yields. The absence of emission features at 9.7 and 18  $\mu\text{m}$  due to silicates is a consequence of the fact that the dust is optically thick at those wavelengths.

#### 4. CIRCUMSTELLAR MATTER

One of the biggest surprises of SN1987A was the observation of its system of three circumstellar rings (Figure 1). The inner equatorial ring (ER) is a circle of radius  $R_{ER} \approx 0.6 \text{ lt-yr}$ , inclined at  $43^{\circ}$  (Sugerman et al. 2005). The faint outer loops are roughly coaxial with the inner ring but not coplanar. They have radii about three times that of the inner ring and their centers are displaced by  $\pm \sim 1.3 \text{ lt-yr}$  along the cylinder axis.

The rings are glowing because they were ionized by the flash of EUV and soft X-rays that lasted a few hours after the supernova blast wave emerged from the photosphere of the progenitor. The luminosity of the ring (Figure 2) increased to a maximum at about 400 days (Fransson et al. 1989; Sonneborn et al. 1997), the time when the ionizing flash illuminated the far side of the ring. Thereafter, the luminosity faded owing to recombination and radiative cooling. Modeling of the evolution of the UV and optical lines shows that a burst with a radiation temperature of  $\gtrsim 10^6 \text{ K}$  is needed to explain the presence of the highest ionization lines of N V (Lundqvist & Fransson 1991, 1996; Mattila et al. 2010). In addition these authors find a strong He and N enrichment, typical of CNO processing. One can also estimate the mass and density of ionized gas in the ER from the luminosity and fading rate of narrow emission lines from the ring. At first, the ring faded rapidly, indicating that the emission was dominated by relatively high density  $n \sim 3 \times 10^4 \text{ cm}^{-3}$  gas, but the fading rate decreased with time, indicating also a lower density component,  $n \sim 1 \times 10^3 \text{ cm}^{-3}$  gas (Mattila et al. 2010). The total mass of gas in the ER that was ionized by the SN flash is  $\sim 0.06 M_{\odot}$ .

Radiation-hydrodynamic models of the shock break-out find a peak temperature of the radiation  $\sim 1.2 \times 10^6 \text{ K}$  with a peak luminosity  $\sim 7 \times 10^{44} \text{ erg s}^{-1}$  and a decay time scale of less than one hour (Ensmann & Burrows 1992; Blinnikov et al. 2000). The equilibrium

assumptions behind this modeling have, however, been criticized by Sapir, Katz & Waxman (2013) and Sapir & Halbertal (2014), who find that the rate of photon creation is not fast enough at the shock breakout, so that a Wien spectrum is formed rather than a blackbody.

The inner ring is expanding with radial velocity  $V_{ER} = 10.3 \text{ km s}^{-1}$ , far too slowly to have been ejected by the supernova explosion. Assuming that the ring expands with constant velocity, one may estimate that it was ejected by the supernova progenitor at a time  $t_{ER} = R_{ER}/V_{ER} \approx 20,000$  years before the explosion.

The origin of the outer rings is not understood. The expansion velocity of these relative to the SN is  $\sim 26 \text{ km s}^{-1}$  (Crotts & Heathcote 2000). Tziamtzis et al. (2011) have analyzed HST and VLT observations and find a distance between these and the SN of between  $1.7 - 2.1 \times 10^{18} \text{ cm}$ . The facts that the outer loops are roughly 2 times farther from the supernova than the ER and are expanding roughly 2.5 as fast suggests that they were ejected at about the same time as the ER (Crotts & Heathcote 2000). The density of the outer rings is estimated to be  $\lesssim 3 \times 10^3 \text{ cm}^{-3}$ , an order of magnitude lower than the highest densities of the ER, but similar to the lower densities dominating the emission at late epochs. In contrast to the ER, the outer rings show a steady decrease in intensity due to the continuing cooling and recombination.

The cylindrical geometry of the triple ring system suggests that the supernova progenitor was a binary star system, and the absence of a star at the explosion site suggests that the stars merged before the explosion. Such a scenario is entirely plausible, given that more than 50% of massive stars belong to close binary systems (Sana et al. 2013). The binary hypothesis also accounts naturally for the fact that the supernova progenitor was a relatively compact blue supergiant, not a red supergiant star. The merger event could expel a loosely bound outer envelope of a red giant progenitor, much as occurs during the formation of bipolar planetary nebulae (Soker 1998). Morris & Podsiadlowski (2007, 2009) have proposed such a merger model for the formation of the triple ring system of SN1987A.

While the merger scenario is a plausible explanation for the origin of the triple ring system, the situation is far from settled. Single star models have been proposed that seem to account for the morphology of the triple ring equally well. For example, Tanaka & Washimi (2002) have proposed a model in which the progenitor is a red supergiant star having a stellar wind with an embedded magnetic field. The field is wrapped into a toroidal field by the stellar rotation, and the resulting pinch effect confines a dense neutral sheet plasma in an equatorial disk. Magnetic pressure also causes a density enhancement at mid-latitudes. After the progenitor makes transition to a blue supergiant, the fast blue supergiant wind inflates a bubble that concentrates the density enhancements of the blue supergiant wind into the triple ring system.

Alternatively, Chita et al. (2008) have proposed a purely hydrodynamic model based on a rapidly rotating  $12 M_{\odot}$  progenitor. The rapid contraction as the star transitions from the red supergiant stage to the blue supergiant stage and a corresponding increase of the rotational velocity at the surface lead to a centrifugal ejection of a flattened torus, which is later compressed into the equatorial ring. The rapid rotation in the BSG stage also leads to a highly anisotropic wind with most of the mass loss and highest wind velocity in the polar direction. The break-out of this wind from the shell expelled by the RSG wind may give rise to a density enhancement at the interface between these components and explain the two outer rings. Whether the same scenario also can be applied to more massive progenitors remains to be seen.

Many uncertainties remain about the distribution of circumstellar matter. For example,

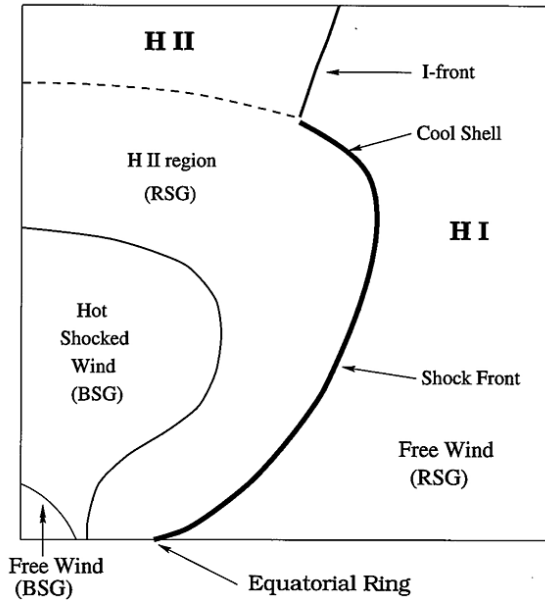


**Figure 8**

Cartoon of the circumstellar medium of Sanduleak -69° 202 before the explosion (Chevalier & Dwarkadas 1995).

how is the structure of the ejected matter modified by the ionizing radiation and stellar wind of the blue supergiant progenitor? To explain the early radio emission Chevalier & Dwarkadas (1995) proposed that the ionizing radiation from the progenitor would produce an HII region of density  $n \approx 10^2 \text{ cm}^{-3}$  bounded on the inside by the shocked stellar wind of the progenitor and on the outside by the ER. **Figure 8** shows a schematic figure of the structure of the circumstellar medium around the progenitor with the interacting winds and the HII region. An upper limit of  $\sim 200 \text{ cm}^{-3}$  for the HII-region was derived from the low flux of N V  $\lambda 1240$  1600-1800 days after the explosion (Lundqvist et al. 1999). Consistent with this, a component with a density of  $\sim 100 \text{ cm}^{-3}$  and mass of  $\sim 0.02 M_{\odot}$  was found to be needed to explain optical lines at  $\sim 5000$  days (Mattila et al. 2010).

Even more mysterious is the distribution of circumstellar matter beyond the triple ring system detected through echoes of the supernova light reflected by dust grains. Sugerman et al. (2005) have constructed a detailed model for the distribution of this matter assuming that it has cylindrical symmetry along the axis of the triple ring system and reflection symmetry about the plane of the ER. The structure has an hourglass shape, having a radius  $\sim 3 \text{ lt-yr}$  in the equatorial plane and extending to  $\sim 20 \text{ lt-yr}$  in the polar directions. The estimated total mass of gas and dust is  $\sim 1.7 M_{\odot}$ . It seems likely that this structure was ejected by the progenitor system some time before the triple ring system; but, as yet, no model has been proposed for its formation. Since no spectral lines were detected from the structure, we have no evidence for its kinematics or age. The fact that the blast wave has now advanced beyond the ER (Sect. 4.2) gives us hope that we will be able to probe this region in the future.



## 4.1. The impact

Soon after the discovery of the circumstellar rings, people realized that a spectacular display would ensue when the supernova blast wave struck the ER. The date when this crash would begin depended on the model for the density structure of the outer envelope of the supernova and on the distribution of circumstellar matter inside the ER. Estimates ranged from ca. 1999 (Luo, McCray & Slavin 1994) to ca. 2005 (Chevalier & Dwarkadas 1995).

In fact, evidence that this crash was beginning first appeared in 1995 as a rapidly brightening hotspot ('Spot1') on the NE quadrant of the ER (Sonneborn et al. 1998; Lawrence et al. 2000). This event was followed a few years later by the appearance of three more spots on the SE quadrant. By January 2003 the ER was fully encircled by hotspots, of which there are now  $\sim 30$  (**Figure 9**).

The spots are moving radially outward, with longitudinal velocities (inferred from Doppler shifts) and transverse velocities (inferred from proper motions) extending up to  $\sim 700 \text{ km s}^{-1}$  (Fransson et al. 2015). Evidently, the hotspots are the result of shocks propagating into dense clumps of gas in the ER.

We interpret the interaction of the supernova with the ER in the context of a schematic model illustrated in **Figure 10**. The central structure represents the nucleosynthesis products and the internal dust. They are surrounded by the freely expanding outer envelope of the supernova composed mostly of hydrogen and helium (rendered blue). This envelope is suddenly decelerated at a reverse shock (the blue-yellow interface) and heated to temperatures  $\sim 10^7 \text{ K}$ . The shocked envelope drives a blast wave into the ER ring, which consists of slowly expanding gas that was photoionized by the ionizing flash from the initial supernova shock breakout (rendered red) and fingers of relatively dense gas (rendered white). As the blast wave overtakes these fingers, transmitted shocks give rise to soft X-ray and optical emission manifested as hotspots, while reflected shocks heat and compress the debris further and give rise to a higher temperature component of X-ray emission.

**Figure 11** shows a recent high dispersion spectrum obtained with the VLT, showing the different spectral components of the ejecta and shock interaction. The broad  $\text{H}\alpha$  wings up to  $\sim 10,000 \text{ km s}^{-1}$  come from neutral hydrogen crossing the reverse shock, while the intermediate component with velocities up to  $\sim 700 \text{ km s}^{-1}$ , seen more clearly in the insert, originates from the shocked clumps in the ring. The narrow lines with  $\text{FWHM} \sim 10 \text{ km s}^{-1}$ , seen most clearly in the [N II] lines, come from the unshocked ring material. Weak emission from the ejecta with  $\text{FWHM} \sim 2000 \text{ km s}^{-1}$  is seen on the blue side of the intermediate velocity  $\text{H}\alpha$  and [N II] lines.

To be visible optically, the shock must be radiative, i.e., the radiative cooling timescale of the shocked gas must be less than the timescale for the shock to propagate through the clump. The cooling time is  $t_{cool} \approx 38(V_s/500 \text{ km s}^{-1})^{3.4}(n_e/10^4 \text{ cm}^{-3})^{-1}$  years. As time progresses, shocks with increasing velocity will therefore become radiative. This can be seen in the maximum width of the  $\text{H}\alpha$  line, which has increased from  $550 \text{ km s}^{-1}$  in 2007 to  $\sim 800 \text{ km s}^{-1}$  in 2013 (Grönningsson et al. 2008, Migotto et al. 2015, *in prep.*). For a given pressure driving the shock, the above condition sets a lower density limit,  $n_{crit} \approx 10^4 \text{ cm}^{-3}$ , for a clump to become radiative (Pun et al. 2002). If the density falls short of this threshold, the shock will heat the clump to temperature  $> 10^6 \text{ K}$ , at which the shocked gas will emit soft X-rays and very little optical radiation (except for faint coronal emission lines from [Fe IX-XIV] (Grönningsson et al. 2006)). Thus, the passage of the blast wave through the ring will illuminate the dense clumps at high contrast, erasing the narrow line emission from the unshocked ring and creating an increasing luminosity of soft X-rays. A hotspot

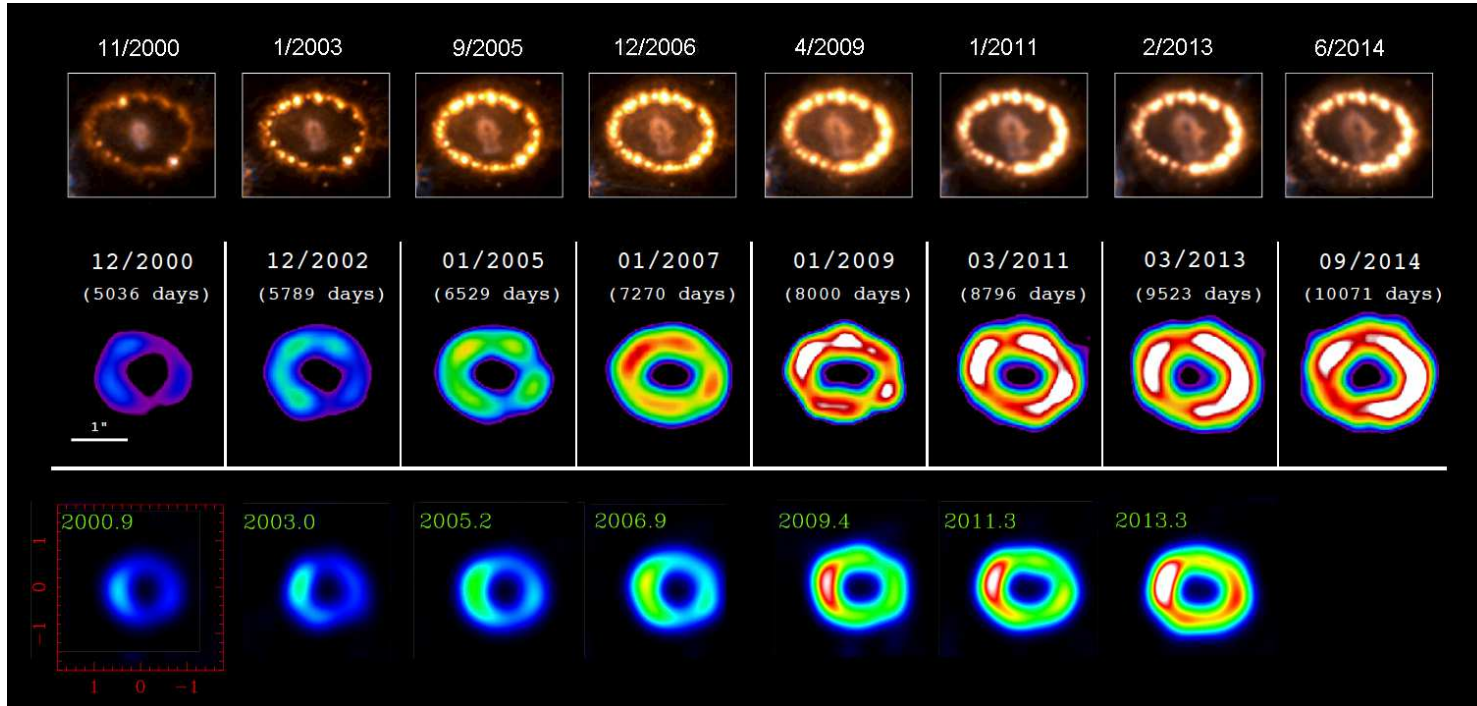


**Figure 9**

Evolution of SN1987A and its Equatorial Ring. Top row – Optical (Fransson et al. 2015). The brightness of the ring has been reduced by a factor of 20 to make it possible to see faint emission from the supernova debris and beyond the ring; Middle row – 0.5 – 3 keV X-rays (Frank et al. 2015, *in prep.*); Bottom row – 9 GHz (Ng et al. 2013).

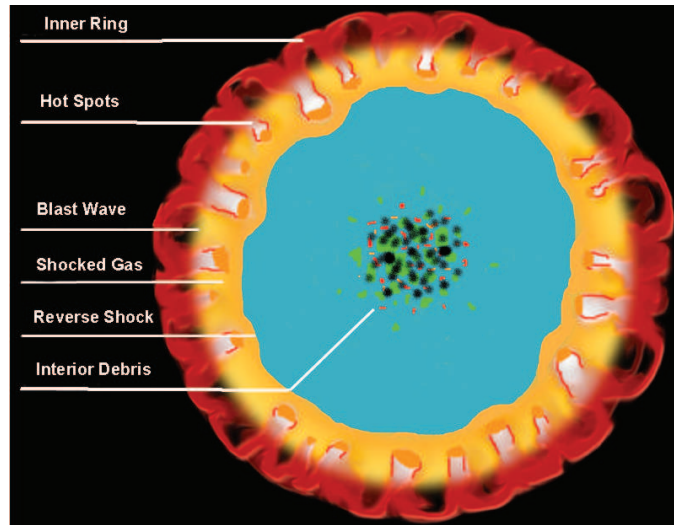


**Figure 10**  
Cartoon illustrating the interaction of the supernova debris with the Equatorial Ring

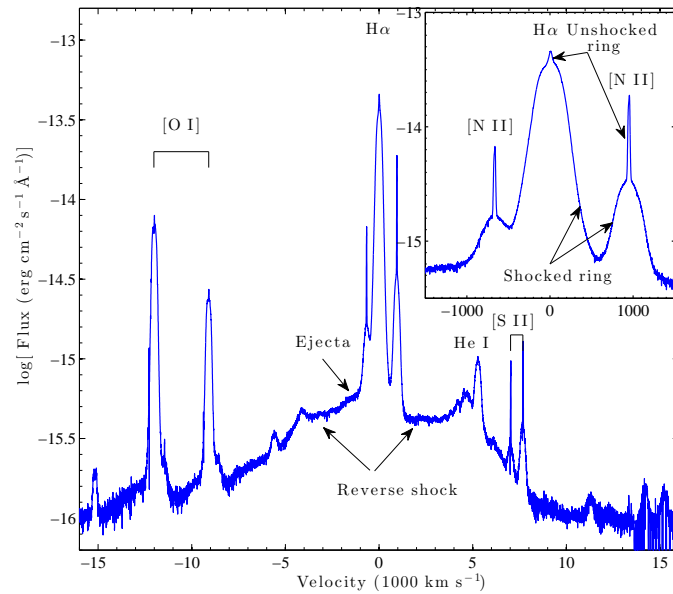


**Figure 11**  
The different spectral components of the ejecta and circumstellar medium interaction as seen in the H $\alpha$  and [N II] lines with UVES/VLT in 2013 (Migotto et al. 2015, *in prep.*). The insert shows a magnification of the  $\pm 1500$  km s $^{-1}$  region around H $\alpha$ . Also the [O I] lines at 6300, 6364 Å have both an ejecta and shocked ring component.

will disintegrate in a timescale comparable to the time for a shock to pass through a clump as a result of hydrodynamic instabilities that shred the cooling layer behind a radiative shock (Pun et al. 2002).

The driving pressure of the shocks propagating into the ring is determined by the ram pressure of the outer envelope of the debris flowing through a reverse shock that lies inside the blast wave. Since the density of this envelope is believed to have a steep gradient,  $\rho \propto r^{-n}$ , where  $n \approx 8.6$ , this pressure will increase with time as  $P \propto t^{3.6}$  if the reverse shock is stationary. It follows that the critical density for the clumps to become radiative will also increase with time, roughly as  $n_{crit} \propto t^2$ . If, as seems plausible, the distribution of clumps is a decreasing function of density, fewer hotspots will appear as time progresses.

This scenario is consistent with observations (Fransson et al. 2015). The light from the hotspots reached a maximum at about 7000 days on the eastern side of the ER and about 8000 days on the western side and then began to fade, while the X-rays continued to increase (Figure 2). A few new hotspots have appeared outside the ring, evidently due to the blast wave overtaking new clumps (Figure 1).

By 1994, before the hotspots appeared, the HST images of the ER were dominated by relatively low density ( $n \sim 10^3 \text{ cm}^{-3}$ ) gas. When they first appeared, the hotspots were found inside the ER, at radial distances typically 5% less than the radius of the ER seen in the HST images (Fransson et al. 2015). This fact is a natural consequence of the action of the progenitor wind on the circumstellar matter, which would push away lower density gas and leave the higher density clumps behind, much as is seen in planetary nebulae such as the Helix Nebula (O’dell & Handron 1996).

The fact that the brightest hotspots lie inside the ER has an interesting implication regarding the distance of SN1987A. In principle, this distance can be determined by dividing the physical diameter of the ring by its angular diameter. The former can be inferred from observations by the IUE satellite of the rise and fall of the narrow line emission from the ring during the first year after the supernova outburst. Panagia et al. (1991) used this technique to estimate that SN1987A was at a distance  $51.2 \pm 3.1 \text{ kpc}$  (*cf.* Gould & Uza (1998)). However, the angular diameter measured from the HST images is that of the ring of low-density gas, while the light curves of the narrow emission lines seen with IUE were probably dominated by emission from the ring of high-density clumps that are now seen as hotspots. If so, the estimated distance to SN1987A should be increased by  $\sim 5\%$ .

## 4.2. The Reverse Shock

The impact of the outer envelope of SN1987A with its circumstellar matter establishes a complex hydrodynamic structure, bounded on the inside by a reverse shock, where the freely expanding outer envelope of the supernova debris is suddenly slowed and heated, and on the outside by a blast wave, where the nearly stationary circumstellar matter is suddenly accelerated. The shapes of the reverse shock surface and the blast wave are determined by the density distribution of circumstellar matter, much of which is uncertain. When the blast wave encounters a density discontinuity, it slows down suddenly and sends a reflected shock back into the shocked gas between the reverse shock and the blast wave. The reflected shock from the equatorial ring will merge with the reverse shock, creating a nearly stationary bow shock and pinching the reverse shock into an hourglass shape. At higher latitudes the shape of the reverse shock is probably determined by the shape of the HII region described by Chevalier & Dwarkadas (1995) (Figure 8).

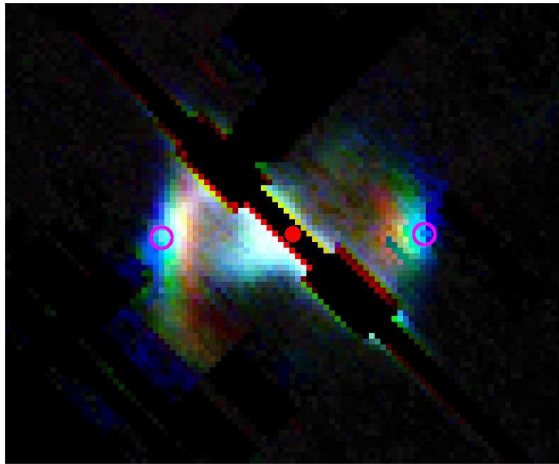


**Figure 12**

Images of  $H\alpha$  emission from reverse shock surface, transformed from STIS spectra (McCray et al. 2015, *in prep.*). Slit ( $0.2''$ ) is centered on supernova (denoted by red dot) and oriented in N/S direction. Horizontal dimension is line-of-sight depth inferred from Doppler shift. The vertical streaks manifest the reverse shock at three epochs: red – 2004; green – 2010; and blue – 2014. The reverse shocks are clearly expanding toward the ER (denoted by red circles). Blue-shifted  $H\alpha$  emission from the inner debris is also evident. Emission from the stationary ring is masked out.

It is possible to map the reverse shock in three dimensions through imaging spectrometry (Figure 12). Hydrogen atoms crossing the reverse shock will emit  $H\alpha$  and  $Ly\alpha$  photons when they encounter the ionized plasma downstream from the shock (Borkowski, Blondin & McCray 1997). The emitted photons will have Doppler shifts corresponding to the freely streaming atoms before they cross the shock, so that Doppler shifts map into depths along the line of sight. It is also possible to infer the flux of HI atoms through the reverse shock surface, since each atom crossing the reverse shock will emit, on average, 1  $Ly\alpha$  and 0.2  $H\alpha$  photons before it is ionized.

Michael et al. (1998, 2003); Heng et al. (2006); France et al. (2010, 2011) and McCray et al. (2015) have employed the Space Telescope Imaging Spectrograph (STIS) to map the reverse shock near the equatorial ring where it is brightest. The main results of these studies are:

1. The  $H\alpha$  emission is dominated by the reverse shock inside the ER, as expected.
2. The observations show substantial departures from cylindrical symmetry, with the near (N) side of the ring brighter than the far (S) side by  $\sim 30\%$ .
3. Near the equatorial ring, the reverse shock surface is moving outward with radial velocity  $\sim 2500 \text{ km s}^{-1}$
4. The flux of  $H\alpha$  photons has increased steadily, by a factor  $\sim 7$  in the interval April 1997 – January 2010.
5. The flux of  $Ly\alpha$  photons has increased more rapidly than that of  $H\alpha$ .
6. In some locations, the photon ratio  $R_{LH} = Ly\alpha/H\alpha$  exceeds the predicted value  $R_{LH} = 5$  by a factor  $> 2$ .
7. Unlike the  $H\alpha$  emission, the  $Ly\alpha$  emission is not confined to the reverse shock surface,

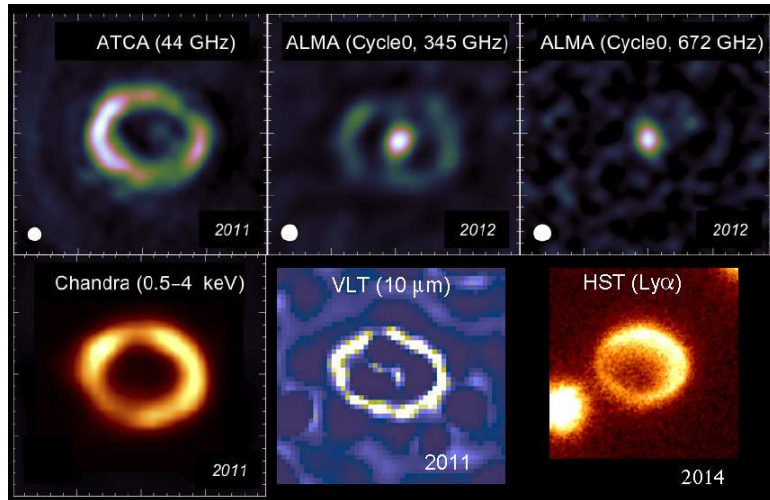


**Figure 13**

Multi-Wavelength Images of SN 1987A: Top row – ATCA & ALMA (Indebetouw et al. 2014); second row – Chandra 0.5 – 4 keV, (Frank et al. 2015, *in prep.*); VLT 10  $\mu\text{m}$ , January 2011 (Bouchet & Danziger 2014); HST Ly $\alpha$ , June 2014 (France et al. 2015).

but is dominated by emission interior to this surface (**Figure 13**).

Far from the equatorial plane, the reverse shock is too faint to see with the STIS. Instead, France et al. (2015) obtained images of this faint emission with the Wide Field Camera of the Hubble Space Telescope in combination with filters that select highly red- and blue-shifted H $\alpha$  emission. An extension of the reverse shock substantially out of the ring plane is consistent with spectra obtained from the VLT (Fransson et al. 2013), which show H $\alpha$  emission extending to  $\gtrsim 10,000 \text{ km s}^{-1}$ , while the maximum velocity in the ring plane is  $\sim 4500(25 \text{ yrs}/t) \text{ km s}^{-1}$ .

If the flux of ionizing photons into the debris exceeds the flux of HI atoms through the reverse shock, it can suppress the H $\alpha$  emission from the reverse shock. Smith et al. (2005) predicted that this suppression may occur sometime around 2015, but we have not yet seen any evidence of this phenomenon (Fransson et al. 2013).

Evidently, the Ly $\alpha$  emission is dominated by a mechanism other than excitation of HI atoms crossing the reverse shock surface. The most likely candidate is thermal excitation by electrons heated by external X-rays penetrating into the unshocked debris. If the debris has ionization fraction  $n_e/n_H > 0.03$ , most of the energy deposited by X-ray photoionization will heat the electrons, and thermal excitation of HI will produce Ly $\alpha$  without much H $\alpha$ , explaining the large observed value of  $R_{LH}$ . The fact that the asymmetry of the Ly $\alpha$  image tracks that of the X-ray image (Figure 13) supports this interpretation.

### 4.3. X-ray Emission

About 4 months after the explosion, the GINGA satellite detected a source of hard ( $\sim 25 \text{ keV}$ ) X-rays from SN1987A. As discussed by McCray (1993), these X-rays emerged from the supernova debris as the result of down-Comptonization of gamma rays from  $^{56}\text{Co}$  decay.

Figure 2 shows the light curve of soft (0.5 – 2 keV) X-rays. They were first detected by ROSAT in Feb 1991 (day 1448) and increased steadily until day 3013 (Hasinger, Aschenbach & Truemper 1996). When first observed with Chandra on day 4608, the soft X-ray flux exceeded a linear extrapolation of the ROSAT light curve by a factor  $\sim 1.6$  (Burrows et al. 2000). Thereafter, the light curve increased exponentially, from  $\approx 10 L_{\odot}$  on day 4300 to  $\approx 500 L_{\odot}$  on day 8600. The light curve appears to have begun to level off since then (Frank et al. 2015, *in prep.*).

The soft X-ray image (Figure 13) is an irregular torus. When first observed with Chandra, it was brightest on the east side, but after the impact was well underway, the image resembled that of the optical hotspots, except that the angular resolution was lower. Before day 6100, the image was expanding with radial velocity  $\sim 8500$  km/s (Racusin et al. 2009); thereafter, the expansion velocity slowed to  $\sim 1850$  km/s (Helder et al. 2013). Evidently, the X-ray emission is related to the same shock system that gives rise to the optical hotspots.

High-resolution X-ray spectra of SN1987A (**Figure 14**) have been obtained with the Chandra Observatory, (Michael et al. 2002; Zhekov et al. 2005, 2006; Dewey et al. 2008) and with the XMM observatory (Sturm et al. 2010). The spectra are dominated by emission lines from K-shell transitions of H- and He-like ions of N, O, Ne, Mg, Si, and S, and L-shell transitions of FeXVII – FeXX (Figure 14). The picture that emerges from the grating spectra is complex. A bimodal distribution function of emission measures vs. temperature, with peaks at  $\approx 0.5$  keV and  $\approx 2.0 - 2.5$  keV, is required to fit the line ratios. (The temperature of the hot component is decreasing with time.) Fitting an expanding ring model to the X-ray line profiles gives a radial expansion velocity  $\sim 300$  km s $^{-1}$ , much less than the value  $\sim 1850$  km s $^{-1}$  inferred from the proper motion of the expanding X-ray image. Evidently, the low-temperature component of the X-ray emission is dominated by shocks transmitted into clumps of relatively high-density gas, (which also produce the optical and UV emission from the radiative shocks), while the high-temperature component is dominated by faster shocks reflected off these clumps. The fact that the expansion velocity deduced from proper motion of the X-ray image exceeds that deduced from the X-ray line profiles suggests that the dense clumps are in fact radial fingers of gas being overtaken by the blast wave.

Orlando et al. (2015) have recently modeled the X-ray evolution from the time of the explosion up to 40 years, using a high resolution adaptive mesh hydrocode. Their 3-d simulation include the ejecta, with clumpiness put in by hand, the wind of the progenitor, an HII region of constant density and an ER (similar to that in Figure 8). The ER includes both clumps of high density and a smooth inter-clump medium of lower density. The adaptive mesh is crucial in order to resolve both the interaction with the clumps at small scales and the large scale interaction with the HII region. From the resulting hydrodynamic structure they calculate the X-ray emission, taking departures from ionization- and electron-ion temperature equilibrium into account.

In **Figure 15** the resulting soft and hard X-ray light curves are shown with contributions from the different components, compared to ROSAT, ASCA, Chandra and XMM observations. The emission up to 15 years is dominated by the interaction with the HII region. When the ejecta starts to interact with the ring this dominates the emission until  $\sim 32$  years. The soft X-rays are dominated by the clumps, while the hard X-rays mainly come from the interaction with the smooth component. In the soft X-rays the contribution from the ring is predicted to peak at  $\sim 27$  years, and at somewhat later time for the hard X-rays. It then declines similar to what is already observed in the optical (Fransson et al.





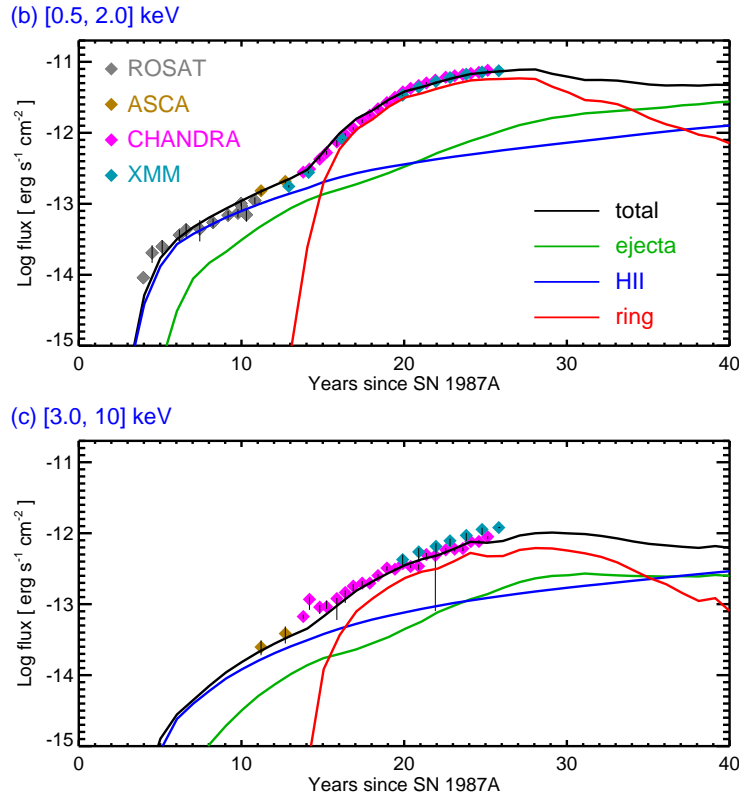


**Figure 15**

Simulation of the soft and hard X-ray evolution of SN 1987A compared to observations (Orlando et al. 2015). The contributions from the different emission components are shown separately for each of these bands.

2015). As discussed earlier, it would not be surprising to find a correlation between the soft X-rays and optical emission from the hotspots. In the final phase, when the blast wave has propagated past the ring, the X-ray emission is mainly coming from the reverse shock, heating the envelope of the ejecta. The morphology in this phase is characterised by bright knots of shocked ejecta clumps.

The parameters of the circumstellar medium and ring for their best fit model agree well with those determined from the optical and X-ray observations. The evolution during the HII region phase is sensitive to the density profile of the ejecta and is best reproduced for a  $\rho \propto V^{-8}$  profile. This is similar to what modeling of the early light curve indicates.

#### 4.4. Dust emission from the ring

If circumstellar gas containing dust grains is heated to temperatures  $\gtrsim 10^6$  K, the dust grains can be heated by collisions with electrons and ions and will radiate this heat as infrared continuum. If the gas has cosmic abundances of refractory elements typical of interstellar gas and a substantial fraction resides in grains, the emission of infrared radiation by the

grains is more efficient than the emission of X-rays by electron-ion collisions. This is the case for many supernova remnants (Dwek & Arendt 1992) and it is true for SN1987A as well.

ISO observations at  $t \sim 3900$  d showed a marginally resolved source at 6.8–14.3  $\mu\text{m}$  (Fischera, Tuffs & Völk 2002a). Both the size and elongation argued for an origin from the region of the ring. Modeling of the spectrum yielded a grain mass of  $\sim (0.5 - 1) \times 10^{-6} M_{\odot}$  and a temperature of  $\sim 200$  K (Fischera, Tuffs & Völk 2002b).

With the Spitzer telescope Bouchet et al. (2006) and Dwek et al. (2008) observed the spectrum of infrared emission from SN1987A in the mid-IR (5–30  $\mu\text{m}$ ) band at two epochs,  $t = 6190$  d and  $t = 7137$  d (Figure 5). Bouchet et al. (2006) and Bouchet & Danziger (2014) also obtained diffraction-limited images of SN1987A at 10  $\mu\text{m}$  (Figure 13) showing clearly that the mid-IR radiation was coincident with the X-ray image.

Dwek et al. (2008) presented a detailed study of this emission and showed that it could be modeled with a plane-parallel shock entering circumstellar gas having density  $\sim 0.3 - 1 \times 10^4 \text{ cm}^{-3}$  containing silicate grains having LMC interstellar abundance ( $\sim 0.3$  times cosmic abundance). Collisions with electrons and ions in the shocked plasma ( $T \approx 3.5 \times 10^6$  K) heat the grains to  $\approx 180$  K. The ratio of mid-IR to X-ray continuum luminosity decreased from  $IR/X = 3.8 \pm 0.6$  at  $t = 6184$  d to  $IR/X = 2.7 \pm 1.0$  at  $t = 6582$  d, evidently due to destruction of the grains by sputtering in the X-ray emitting plasma (Dwek et al. 2010, Figure 2). Dwek et al. also find evidence that dust grains smaller than  $\sim 0.02 \mu\text{m}$  were evaporated by the initial UV/soft X-ray flash (Fischera, Tuffs & Völk 2002b).

#### 4.5. Radio emission

SN 1987A has been observed since the event with the Molonglo Observatory Synthesis Telescope (MOST Turtle et al. 1990; Ball et al. 2001) at 36 cm, and with the Australia Telescope Compact Array (ATCA) at 3 – 20 cm since mid–1990, (e.g. Manchester et al. 2002; Zanardo et al. 2010; Ng et al. 2013). The radio remnant has been imaged with ATCA at 3 mm by (Lakićević et al. 2012a) and, more recently, at 3.2 mm and 450  $\mu\text{m}$  with the ALMA array (Indebetouw et al. 2014; Zanardo et al. 2014).

The radio remnant appears as a torus; however, its evolution and morphology differ substantially from the optical and X-ray images (Figure 9). From day  $\sim 5000$  to day  $\sim 8000$ , the radio luminosity at 3 – 35 cm (Figure 2) increased exponentially with an  $e$ -folding time of  $2408 \pm 227$  days (Zanardo et al. 2010). Since then, the radio remnant has continued to brighten, but at a slower rate (Staveley-Smith et al. 2014). In contrast to the X-rays, no sharp break in the radio light curve was evident at  $t \sim 6000$  d, when the optical hotspots appeared. Likewise, the radial expansion velocity of the radio image did not decelerate rapidly when the optical hotspots appeared, but remained approximately constant at  $\sim 4000$  km/s (Ng et al. 2008).

The radio image has remained brighter on the east side (Ng et al. 2013), unlike the optical and X-ray images which have become brighter on the west (Figure 9). The radio emission is evidently synchrotron radiation. It has a power law spectrum (Figure 5),  $S_{\nu} \propto \nu^{-\alpha}$ , where the overall spectral index has evolved from  $\alpha = 0.91$  at day 1517 to  $\alpha = 0.73$  at day 9280.

The power law spectrum of synchrotron radiation is believed to be the result of diffusive acceleration of relativistic electrons across a shock. According to the simplest version of this theory (e.g., Jones & Ellison 1991), the synchrotron spectral index is related to the

shock compression ratio,  $\sigma$ , by  $\alpha = 3/[2(\sigma - 1)]$ . For a high Mach number shock such as the supernova blast wave,  $\sigma = 4$ , hence  $\alpha = 0.5$ . The fact that the observed spectral index is steeper than this requires some modification of this theory. The situation is still unclear. One possible explanation is that the shock compression ratio,  $\sigma < 4$ . This might be the case if the electrons are accelerated primarily by the reflected shocks responsible for the hard X-ray emission. (For example, a plane parallel shock from a blast wave reflected off a dense obstacle will have  $M = 5^{1/2}$  and  $\sigma = 2.5$ , hence  $\alpha = 1$ ). Alternatively, the blast wave may be cushioned by a magnetic field. Another possibility (Kirk, Duffy & Gallant 1996) is that the electrons undergo sub-diffusion in a turbulent magnetic field, in which case  $\alpha = 9/[4(\sigma - 1)]$ , which implies  $\alpha = 0.75$  for  $\sigma = 4$ .

Clearly, the relativistic electrons in SN 1987A are accelerated in a different environment from that responsible for the optical and X-ray emission. One might conjecture that the injection of relativistic electrons has greater efficiency in a low-density environment than in the higher density environment favored by the optical and X-ray emission. The brighter emission on the eastern lobe may be the result of a smaller fraction of injected particles than on the west.

The spectral analysis of ATCA and ALMA images from 7 mm to 870  $\mu\text{m}$  shows  $0.1 \lesssim \alpha \lesssim 0.4$  across the western regions of the remnant (Zanardo et al. 2014), which might be attributed to particle flux injection by a possible pulsar (Gaensler & Slane 2006). This interpretation must be regarded as tentative, however, given the contribution by thermal emission from cold dust in this band.

Potter et al. (2014) have developed an ambitious model to account for the evolution and morphology of the non-thermal emission from SN1987A. The model consists of a hydrodynamic simulation of the supernova explosion encountering a circumstellar environment similar to that proposed by (Chevalier & Dwarkadas 1995). By incorporating semi-analytic recipes for diffusive shock acceleration and magnetic field amplification into the hydrodynamic solutions and choosing parameters for the pre-supernova environment, the authors are able to produce models that fit the evolution of the radio image reasonably well. An asymmetric supernova explosion is required to account for the E/W asymmetry of the radio image. The model does not account for the evolution of the spectral index, however.

#### 4.6. VHE gamma-rays

Based on the ATCA radio observations Berezhko, Ksenofontov & Völk (2011) and Dwarkadas (2013) have predicted the expected TeV gamma rays resulting from the  $\pi^0$  decay, resulting from the interaction of the cosmic rays at the shocks with the protons in the circumstellar medium. Depending on assumptions about the circumstellar medium properties the expected flux was  $\sim 2.5 \times 10^{-13}$  photons  $\text{cm}^{-2} \text{s}^{-1}$  (Berezhko, Ksenofontov & Völk 2011) and  $\sim 8 \times 10^{-14}$  photons  $\text{cm}^{-2} \text{s}^{-1}$  (Dwarkadas 2013).

The region around SN 1987A has recently been observed with the H.E.S.S. gamma-ray telescope (Abramowski et al. 2015). While they find emission from nearby pulsar wind nebulae, young supernova remnants and stellar wind bubbles, SN 1987A only yielded an upper limit of  $< 5 \times 10^{-14}$  photons  $\text{cm}^{-2} \text{s}^{-1}$  above 1 TeV, lower than the above predictions. There are, however, a number of uncertainties in the latter, in particular the proton injection rate, the non-thermal proton-to-electron ratio, magnetic field and the geometry and parameters of the shocks. Nevertheless, this shows that these observations in combination with the radio and hard X-ray observations can put interesting constraints on

the efficiency of cosmic ray acceleration. For SN 1987A Abramowski et al. (2015) estimate that less than 1% of the explosion energy is in cosmic rays.

Recently, Berezhko, Ksenofontov & Völk (2015) have revised their model to better comply with the observed structure and parameters of the circumstellar medium. In particular, the mass of the equatorial ring was decreased by an order of magnitude. With this change the model flux decreased to close to the upper limit observed with H.E.S.S..

## 5. HOW UNIQUE WAS SN 1987A?

The discovery that the progenitor of SN 1987A was a blue supergiant rather than a red supergiant came as a big surprise. Since then several cases of SNe with similar light curves and luminosities have been discovered.

Some 18 SNe have been identified with light curves similar to SN 1987A (Kleiser et al. 2011; Pastorello et al. 2012; Taddia et al. 2012; Arcavi et al. 2012; González-Gaitán et al. 2015; Shivvers et al. 2016). Because of the limited sample and their intrinsic faintness the rate of these events is highly uncertain. Pastorello et al. (2012) estimate a rate of 1-3 % of all core collapse SNe to be photometrically similar to SN 1987A, similar to the estimate by Kleiser et al. (2011). Likewise, Shivvers et al. (2016) find 2 SNe with light curves resembling SN1987A among 135 core collapse supernovae in a volume-limited sample assembled from the Lick Observatory Supernova Search (Li et al. 2011).

An important clue to the nature of the blue progenitor may be the metallicity of the host environment. Early models showed that a low metallicity indeed could lead to a blue progenitor (Arnett et al. 1989). A recent study of SNe with light curves indicating a BSG progenitor by Taddia et al. (2013) shows that most of these occur in low metallicity environments such as low-luminosity galaxies or at large distances from the nuclei of luminous hosts. (There are also cases with near solar metallicity.) As shown in **Figure 16** the metallicities are clearly different from those of the Type IIP SNe, but similar to that of the Type IIb SNe.

There are several stars in our galaxy that are known to have ring systems resembling SN 1987A. The best studied are Sher-25, HD168625 and SBW1 (Brandner et al. 1997; Nota et al. 1996; Smith 2007; Smith et al. 2013). All three have equatorial rings with similar dimensions to SN 1987A. For SBW1 an hourglass structure emanating from the ring is seen, which may resemble the one which may be present in SN 1987A (Smith et al. 2013, **Figure 17**). The dust emission seen in the interior of the ring would be evaporated by the flash of EUV and soft X-rays at the time of the shock breakout (Fischera, Tuffs & Völk 2002b). HD168625 is an LBV with a ring system which closely resembles that of SN 1987A, including both an equatorial and two polar rings. The expansion velocities of the rings of these three objects are  $\sim 20 \text{ km s}^{-1}$ , twice as high as for the inner ring of SN 1987A, but similar to the outer rings.

In the case of Sher-25 the star has a luminosity considerably greater,  $\log L = 5.9 \pm 0.2 L_{\odot}$  (corresponding to a  $\sim 60 M_{\odot}$  ZAMS star), than Sanduleak -69° 202 with  $\log L = 5.1 L_{\odot}$ . HD168625 has a variable luminosity of  $\log L = 5.0 - 5.4 L_{\odot}$  (Nota et al. 1996). SBW1 is only somewhat more luminous than the progenitor of SN 1987A, with spectral types B 1.5Iab and B 3Ib, respectively, and may therefore in this respect be the star closest to the SN 1987A progenitor.

Neither of these cases shows the large N/O ratio expected for a progenitor which has gone through a RSG phase. Lamers et al. (2001) find that RSG's should have surface

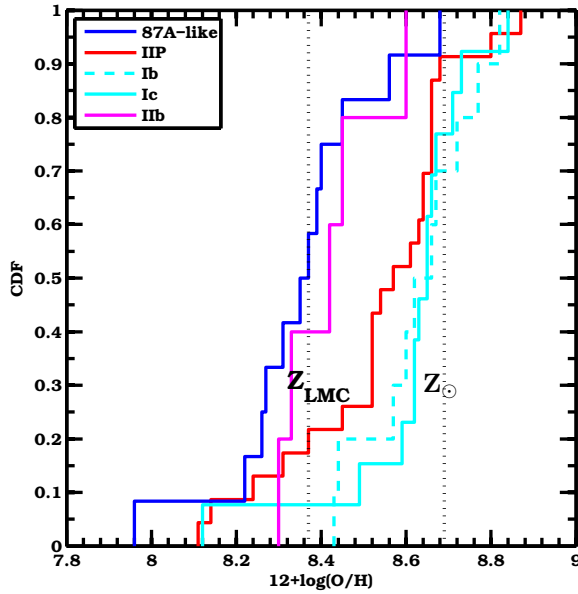


**Figure 16**  
 Cumulative distribution of the metallicity of the environment of Type II SNe with blue supergiant progenitors compared to distributions of Type IIP, Ib and Ic SNe (Taddia et al. 2013)

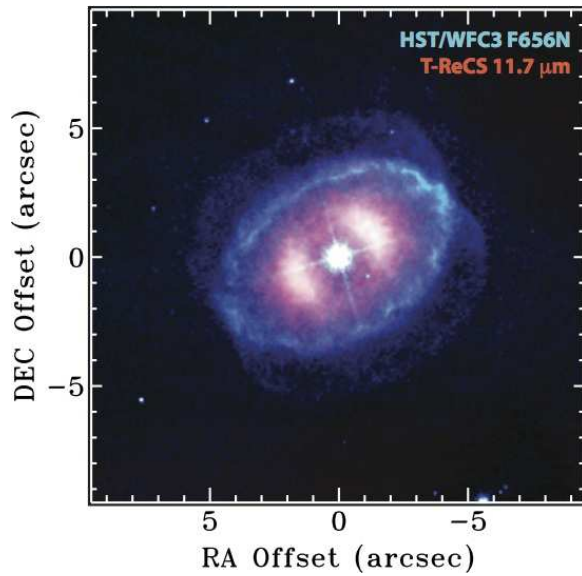


**Figure 17**  
 Composite image of the HST/WFC3 H $\alpha$  image (blue/green), and the Gemini South T-ReCS 11.7  $\mu\text{m}$  image (red/orange) of SBW1 (Smith et al. 2013). Note the hour glass structure in H $\alpha$  above and below the ring and the dust emission from the interior.

abundances in the range  $N/C = 6-30$  and  $N/O=3-20$ , while Sher-25 has  $N/O = 0.36$ , and also the others have moderate N enrichments (Smartt et al. 2002; Smith et al. 2013). For SN 1987A modeling of the IUE observations give  $N/C= 5.0 \pm 2.0$  and  $N/O= 1.1 \pm 0.4$  (Lundqvist & Fransson 1996). Based on the low N enrichment, circumstellar structure and other reasons Smith (2007) has argued that the progenitor of SN 1987A may have been a low luminosity LBV, rather than a star which has passed the RSG phase.

Finally, we remark that while some properties, in particular the blue supergiant progenitor and the circumstellar medium, are unique to this class of supernovae, other aspects are typical for core collapse supernovae. This includes most of the core properties, like the neutrino burst, radioactivity and general nucleosynthesis, hydrodynamics and dust formation. SN 1987A therefore still stands out as the most important object for understanding the physics of core collapse supernova.

## 6. THE FUTURE

We have learned more about supernovae from SN1987A than from any other supernova, but we still have much to learn. Here are a few of the outstanding questions.

**Do we understand the explosion mechanism?** From observations of ions and molecules we have well determined masses of the most abundant isotopes, good estimates of the masses and some information on morphology of the most abundant elements in the ejecta. Much of this has been obtained thanks to new instruments and telescopes that have become available during the last decade.

On the theoretical side there has been much progress both in incorporating more realistic physics and in more powerful computing resources. Still, there is a lack of models that can be directly compared to the observations. Most explosion models are only calculated up to a few seconds and the connection between the structure and nucleosynthesis at this epoch to what is observed when the core has become transparent is not well understood. Some steps in this direction have been taken (e.g., Wongwathanarat, Müller & Janka 2015; Utrobin et al. 2014), but these are more exceptions than a rule. A major uncertainty in the theoretical simulations stems from the distribution of products of nucleosynthesis prior to the explosion, which may be scrambled by violent convection in the late stages of pre-supernova burning.

**How are the newly formed elements distributed throughout the supernova debris?** We can be confident that we will make substantial progress in unraveling its mysteries, thanks in part to the evolution of the supernova itself and also in large part to the dramatic advances in astronomical instrumentation.

We have learned that most of the nucleosynthesis products are confined within a sphere expanding with velocity  $\approx 1500 \text{ km s}^{-1}$  and are mixed macroscopically but not microscopically. With ALMA, we have seen that CO and SiO have different distributions within this volume. In the next few years, we will be able to map the 3-dimensional distribution of CO and SiO with angular resolution an order of magnitude better than heretofore.

SINFONI gives a complementary view of the inner ejecta, which reflects the atomic constituent of the processed material. It is important to note that while the rotational transitions in the sub-mm range are excited by thermal collisions, the NIR lines are excited by the non-thermal excitations from the  $^{44}\text{Ti}$  decay. Further, the sub-mm lines are unaffected by the dust. The NIR emission may still be affected by dust absorption and may be compared to the sub-mm emission observed by ALMA to provide a view of the 3-d dust

distribution.

In the next decade, the GMT and E-ELT, with their enormous collecting area and superior resolution, will provide an even better 3-d view of the ejecta at a time when the X-ray illumination from the ring interaction may reach the inner parts of the core. The James Webb Space Telescope will enable us to search for the mid-IR [Fe II] 26  $\mu\text{m}$  and Fe I 24  $\mu\text{m}$  lines with better resolution and sensitivity.

We also know, from the early emergence of X-rays and gamma rays, as well as the wings of the [Fe II] lines (Spyromilio, Meikle & Allen 1990; Haas et al. 1990), that some of the newly formed elements extend beyond the 1500  $\text{km s}^{-1}$  sphere (McCray 1993). As the debris continues to expand, the X-rays from the impact will penetrate deeper into the debris, eventually causing the debris to glow with optical/IR spectra characteristic of these elements. At some uncertain time in the next few decades, the reverse shock will encounter newly formed elements, particularly the iron bubbles (Li, McCray & Sunyaev 1993) and deform rapidly, as illustrated in simulations by Blondin, Borkowski & Reynolds (2001). Such an event will be accompanied by a rapid change in the X-ray spectrum of the shocked gas.

**What is the history of mass ejection by the progenitor?** The history of mass loss from the progenitor is imprinted on the distribution and kinematics of circumstellar matter. The mass of the visible equatorial ring inferred from observations,  $M_i \sim 0.05 M_\odot$  (Lundqvist & Fransson 1996), is probably limited by the total number of ionizing photons from the initial flash of the supernova. The recent appearance of new hotspots is evidence that we are now beginning to see heretofore invisible matter beyond the ER. Such matter will continue to brighten, steadily as it is ionized by X-rays from the shocked gas and more suddenly as the blast wave overtakes it. Moreover, the evolution of the remnant of SN1987A will be determined by its distribution. Up to now, we can see that only a small fraction of the kinetic energy of the ejecta has been converted to radiation through the impact with this matter. This fraction will approach unity only when the blast wave has overtaken a mass comparable to that of the ejecta. As we have seen, most of this conversion is presently taking place where the blast wave is striking the equatorial ring. We do not know how much mass lies beyond the visible ring. If it is substantial (i.e.,  $\sim M_\odot$ ), the reverse shock will continue to dig into the ejecta in the equatorial plane and will reach the inner ( $V \lesssim 2000 \text{ km s}^{-1}$ ) nucleosynthesis products by  $t \sim 1$  century. At roughly the same time, the blast wave will strike the outer loops and cause them to brighten. On the other hand, if the blast wave has overtaken most of the equatorial ring, the pressure driving the reverse shock will diminish and it will take longer for it to reach the nucleosynthesis products. In any case, it seems likely that the morphology of the remnant of SN1987A will be determined by the history of mass loss by the progenitor for several centuries.

Deep imaging and spectroscopy with the HST, ground-based optical/IR telescopes, Chandra, and eventually with the James Webb Space Telescope (JWST), will give us the clues we need to reconstruct this history. Comparisons with other SN1987A-like supernovae and progenitor systems may give additional insight into the progenitor evolution.

**How are relativistic electrons and cosmic rays accelerated in supernova shocks?** The non-thermal (mm to cm) radiation from SN1987A gives us our first chance to observe acceleration of relativistic electrons by supernova shocks in real time. We have already seen that the morphology and evolution of this radiation differ substantially from those of the optical and X-ray emission from the shocked gas. With ALMA, we will soon be able to obtain images of the non-thermal radiation and its polarization with angular

resolution better than  $0.1''$ . Optical images and spectra of comparable resolution from HST will enable us to characterize the physical conditions in the shocks where the relativistic electrons are accelerated. On a longer time scale the Cherenkov Telescope Array (CTA) will improve the sensitivity of H.E.S.S. for TeV gamma rays by an order of magnitude, which should challenge the predictions for cosmic ray production in SN 1987A (Sect. 4.6).

**What is the compact object?** The initial burst of neutrinos from SN1987A is compelling evidence that a compact object was formed during its core collapse (Arnett et al. 1989). The object is most likely a neutron star, but it is possible that continued infall triggered a further collapse to a black hole.

Despite intensive efforts, using the most sensitive available instruments spanning the entire electromagnetic spectrum, astronomers have been unable to detect any signal from the compact object since the neutrino burst. Little has changed since McCray (2007) reviewed the situation. The upper limit to the luminosity of the compact object is a few tens of  $L_{\odot}$ . Graves et al. (2005) find an upper limit of only  $\sim 1.3 L_{\odot}$  between 2900-9650 Å. The dust we know is present in the core may, however, convert any emission in the UV, optical and NIR ranges from a pulsar wind nebula to the far-IR range.

The expectation that we might find a bright compact object at the center of SN1987A has been dampened a bit by the observations that several supernova remnants, notably Cas A, have compact sources with X-ray luminosity less than a few  $L_{\odot}$  and no radio emission de Luca (2008). Evidently, these sources are cooling neutron stars with very weak magnetic fields. If SN1987A contained such a neutron star, it would have not have been detected up to now.

Our best hope to detect the compact object is to image SN1987A with higher angular resolution than heretofore. Soon it will be possible with ALMA to search for a compact flat spectrum radio source near the center of the explosion debris or a compact component to the thermal dust emission.

## ACKNOWLEDGMENTS

We thank the following people for advice and assistance with this review: Adam Burrows, David Burrows, Pete Challis, Roger Chevalier, Eli Dwek, Kari Frank, Anders Jerkstrand, Patrick Kelly, Josefin Larsson, Peter Lundqvist, Mikako Matsuura, Katia Migotto, Francesco Taddia and Giovanna Zanardo. The research of CF is supported by the Swedish Research Council and Swedish National Space Board.

## LITERATURE CITED

- Abramowski A, Aharonian F, Ait Benkhali F, Akhperjanian AG, Angüner EO, et al. 2015. *Science* 347:406–412
- Arcavi I, Gal-Yam A, Cenko SB, Fox DB, Leonard DC, et al. 2012. *Astrophys. J.* 756:L30
- Arnett WD, Bahcall JN, Kirshner RP, Woosley SE. 1989. *Annual Review of Astronomy and Astrophysics* 27:629–700
- Axelrod TS. 1980. *Late time optical spectra from the Ni-56 model for Type 1 supernovae*. Ph.D. thesis, California Univ., Santa Cruz.
- Ball L, Crawford DF, Hunstead RW, Klammer I, McIntyre VJ. 2001. *Astrophys. J.* 549:599–607
- Berezhko EG, Ksenofontov LT, Völk HJ. 2011. *Astrophys. J.* 732:58
- Berezhko EG, Ksenofontov LT, Völk HJ. 2015. *ArXiv e-prints*
- Blinnikov S, Lundqvist P, Bartunov O, Nomoto K, Iwamoto K. 2000. *Astrophys. J.* 532:1132–1149



- Blondin JM, Borkowski KJ, Reynolds SP. 2001. *Astrophys. J.* 557:782–791
- Boggs SE, Harrison FA, Miyasaka H, Grefenstette BW, Zoglauer A, et al. 2015. *Science* 348:670–671
- Borkowski KJ, Blondin JM, McCray R. 1997. *Astrophys. J.* 476:L31–L34
- Bouchet P, Danziger J. 2014. *9500 Nights of Mid-Infrared Observations of SN 1987A: the birth of the remnant*. In *IAU Symposium*, eds. A Ray, RA McCray, vol. 296 of *IAU Symposium*
- Bouchet P, Dwek E, Danziger J, Arendt RG, De Buizer IJM, et al. 2006. *Astrophys. J.* 650:212–227
- Brandner W, Chu YH, Eisenhauer F, Grebel EK, Points SD. 1997. *Astrophys. J.* 489:L153–L156
- Burrows A. 2013. *Reviews of Modern Physics* 85:245–261
- Burrows DN, Michael E, Hwang U, McCray R, Chevalier RA, et al. 2000. *Astrophys. J.* 543:L149–L152
- Chevalier RA, Dwarkadas VV. 1995. *Astrophys. J.* 452:L45–L48
- Chita SM, Langer N, van Marle AJ, García-Segura G, Heger A. 2008. *Astron. Astrophys.* 488:L37–L41
- Chugai NN, Chevalier RA, Kirshner RP, Challis PM. 1997. *Astrophys. J.* 483:925–940
- Couch SM, Chatzopoulos E, Arnett WD, Timmes FX. 2015. *Astrophys. J.* 808:L21
- Crotts APS, Heathcote SR. 2000. *Astrophys. J.* 528:426–435
- de Kool M, Li H, McCray R. 1998. *Astrophys. J.* 503:857–876
- de Luca A. 2008. *Central Compact Objects in Supernova Remnants*. In *40 Years of Pulsars: Millisecond Pulsars, Magnetars and More*, eds. C Bassa, Z Wang, A Cumming, VM Kaspi, vol. 983 of *American Institute of Physics Conference Series*
- Dessart L, Hillier DJ. 2010. *Mon. Not. Roy. Astron. Soc.* 405:2141–2160
- Dewey D, Zhekov SA, McCray R, Canizares CR. 2008. *Astrophys. J.* 676:L131–L134
- Dwarkadas VV. 2013. *Mon. Not. Roy. Astron. Soc.* 434:3368–3377
- Dwek E, Arendt RG. 2015. *ArXiv e-prints*
- Dwek E, Arendt RG, Bouchet P, Burrows DN, Challis P, et al. 2008. *Astrophys. J.* 676:1029–1039
- Dwek E, Arendt RG, Bouchet P, Burrows DN, Challis P, et al. 2010. *Astrophys. J.* 722:425–434
- Ensmann L, Burrows A. 1992. *Astrophys. J.* 393:742–755
- Fischera J, Tuffs RJ, Völk HJ. 2002a. *Astron. Astrophys.* 386:517–530
- Fischera J, Tuffs RJ, Völk HJ. 2002b. *Astron. Astrophys.* 395:189–200
- France K, McCray R, Fransson C, Larsson J, Frank KA, et al. 2015. *Astrophys. J.* 801:L16
- France K, McCray R, Heng K, Kirshner RP, Challis P, et al. 2010. *Science* 329:1624–1627
- France K, McCray R, Penton SV, Kirshner RP, Challis P, et al. 2011. *Astrophys. J.* 743:186
- Fransson C, Cassatella A, Gilmozzi R, Kirshner RP, Panagia N, et al. 1989. *Astrophys. J.* 336:429–441
- Fransson C, Kozma C. 1993. *Astrophys. J.* 408:L25–L28
- Fransson C, Kozma C. 2002. *New A. Rev.* 46:487–492
- Fransson C, Larsson J, Migotto K, Pesce D, Challis P, et al. 2015. *Astrophys. J.* 806:L19
- Fransson C, Larsson J, Spyromilio J, Chevalier R, Gröningsson P, et al. 2013. *Astrophys. J.* 768:88–110
- González-Gaitán S, Tominaga N, Molina J, Galbany L, Bufano F, et al. 2015. *Mon. Not. Roy. Astron. Soc.* 451:2212–2229
- Gould A, Uza O. 1998. *Astrophys. J.* 494:118–124
- Graves GJM, Challis PM, Chevalier RA, Crotts A, Filippenko AV, et al. 2005. *Astrophys. J.* 629:944–959
- Grebenev SA, Lutovinov AA, Tsygankov SS, Winkler C. 2012. *Nature* 490:373–375
- Gröningsson P, Fransson C, Leibundgut B, Lundqvist P, Challis P, et al. 2008. *Astron. Astrophys.* 492:481–491
- Gröningsson P, Fransson C, Lundqvist P, Nymark T, Lundqvist N, et al. 2006. *Astron. Astrophys.* 456:581–589
- Haas MR, Erickson EF, Lord SD, Hollenbach DJ, Colgan SWJ, Burton MG. 1990. *Astrophys. J.* 360:257–266

- Hammer NJ, Janka HT, Müller E. 2010. *Astrophys. J.* 714:1371–1385
- Hanuschik RW, Thimm GJ. 1990. *Astron. Astrophys.* 231:77–84
- Hashimoto M, Nomoto K, Shigeyama T. 1989. *Astron. Astrophys.* 210:L5–L8
- Hasinger G, Aschenbach B, Truemper J. 1996. *Astron. Astrophys.* 312:L9–L12
- Helder EA, Broos PS, Dewey D, Dwek E, McCray R, et al. 2013. *Astrophys. J.* 764:11
- Heng K, McCray R, Zhekov SA, Challis PM, Chevalier RA, et al. 2006. *Astrophys. J.* 644:959–970
- Herant M, Benz W. 1991. *Astrophys. J.* 370:L81–L84
- Herant M, Benz W, Colgate S. 1992. *Astrophys. J.* 395:642–653
- Herant M, Benz W, Hix WR, Fryer CL, Colgate SA. 1994. *Astrophys. J.* 435:339–361
- Indebetouw R, Matsuura M, Dwek E, Zanardo G, Barlow MJ, et al. 2014. *Astrophys. J.* 782:L2
- Jäger C, Dorschner J, Mutschke H, Posch T, Henning T. 2003. *Astron. Astrophys.* 408:193–204
- Janka HT. 2012. *Annual Review of Nuclear and Particle Science* 62:407–451
- Janka HT, Hanke F, Hüdepohl L, Marek A, Müller B, Obergaulinger M. 2012. *Progress of Theoretical and Experimental Physics* 2012:010000
- Jerkstrand A, Fransson C, Kozma C. 2011. *Astron. Astrophys.* 530:A45
- Jones FC, Ellison DC. 1991. *Space Sci. Rev.* 58:259–346
- Kamenetzky J, McCray R, Indebetouw R, Barlow MJ, Matsuura M, et al. 2013. *Astrophys. J.* 773:L34
- Kirk JG, Duffy P, Gallant YA. 1996. *Astron. Astrophys.* 314:1010–1016
- Kjær K, Leibundgut B, Fransson C, Jerkstrand A, Spyromilio J. 2010. *Astron. Astrophys.* 517:A51
- Kleiser IKW, Poznanski D, Kasen D, Young TR, Chornock R, et al. 2011. *Mon. Not. Roy. Astron. Soc.* 415:372–382
- Kozma C, Fransson C. 1992. *Astrophys. J.* 390:602–621
- Kozma C, Fransson C. 1998a. *Astrophys. J.* 496:946–966
- Kozma C, Fransson C. 1998b. *Astrophys. J.* 497:431–457
- Lakićević M, van Loon JT, Stanke T, De Breuck C, Patat F. 2012a. *Astron. Astrophys.* 541:L1–??
- Lakićević M, Zanardo G, van Loon JT, Staveley-Smith L, Potter T, et al. 2012b. *Astron. Astrophys.* 541:L2
- Lamers HJGLM, Nota A, Panagia N, Smith LJ, Langer N. 2001. *Astrophys. J.* 551:764–780
- Larsson J, Fransson C, Kjaer K, Jerkstrand A, Kirshner RP, et al. 2013. *Astrophys. J.* 768:89
- Larsson J, Fransson C, Östlin G, Gröningsson P, Jerkstrand A, et al. 2011. *Nature* 474:484–486
- Lawrence SS, Sugerman BE, Bouchet P, Crotts APS, Uglesich R, Heathcote S. 2000. *Astrophys. J.* 537:L123–L126
- Li H, McCray R. 1993. *Astrophys. J.* 405:730–737
- Li H, McCray R. 1996. *Astrophys. J.* 456:370–383
- Li H, McCray R, Sunyaev RA. 1993. *Astrophys. J.* 419:824–836
- Li W, Leaman J, Chornock R, Filippenko AV, Poznanski D, et al. 2011. *Mon. Not. Roy. Astron. Soc.* 412:1441–1472
- Liu W, Dalgarno A. 1995. *Astrophys. J.* 454:472–479
- Liu W, Dalgarno A, Lepp S. 1992. *Astrophys. J.* 396:679–685
- Lundqvist P, Fransson C. 1991. *Astrophys. J.* 380:575–592
- Lundqvist P, Fransson C. 1996. *Astrophys. J.* 464:924–942
- Lundqvist P, Sollerman J, Kozma C, Larsson B, Spyromilio J, et al. 1999. *Astron. Astrophys.* 347:500–507
- Luo D, McCray R, Slavin J. 1994. *Astrophys. J.* 430:264–276
- Manchester RN, Gaensler BM, Wheaton VC, Staveley-Smith L, Tzioumis AK, et al. 2002. *PASA* 19:207–221
- Matsuura M, Dwek E, Barlow MJ, Babler B, Baes M, et al. 2015. *Astrophys. J.* 800:50
- Matsuura M, Dwek E, Meixner M, Otsuka M, Babler B, et al. 2011. *Science* 333:1258–1261
- Mattila S, Lundqvist P, Gröningsson P, Meikle P, Stathakis R, et al. 2010. *Astrophys. J.* 717:1140–1156

- McCray R. 1993. *Annual Review of Astronomy and Astrophysics* 31:175–216
- McCray R. 2007. *Supernova 1987A at Age 20*. In *Supernova 1987A: 20 Years After: Supernovae and Gamma-Ray Bursters*, eds. S Immler, K Weiler, R McCray, vol. 937 of *American Institute of Physics Conference Series*
- Michael E, McCray R, Chevalier R, Filippenko AV, Lundqvist P, et al. 2003. *Astrophys. J.* 593:809–830
- Michael E, McCray R, Pun CSJ, Borkowski K, Garnavich P, et al. 1998. *Astrophys. J.* 509:L117–L120
- Michael E, Zhekov S, McCray R, Hwang U, Burrows DN, et al. 2002. *Astrophys. J.* 574:166–178
- Morris T, Podsiadlowski P. 2007. *Science* 315:1103–1105
- Morris T, Podsiadlowski P. 2009. *Mon. Not. Roy. Astron. Soc.* 399:515–538
- Ng CY, Gaensler BM, Staveley-Smith L, Manchester RN, Kesteven MJ, et al. 2008. *Astrophys. J.* 684:481–497
- Ng CY, Zanzardo G, Potter TM, Staveley-Smith L, Gaensler BM, et al. 2013. *Astrophys. J.* 777:131
- Nisenson P, Papaliolios C, Karovska M, Noyes R. 1987. *Astrophys. J.* 320:L15–L18
- Nota A, Pasquali A, Clampin M, Pollacco D, Scuderi S, Livio M. 1996. *Astrophys. J.* 473:946–962
- O’dell CR, Handron KD. 1996. *Astronom. J.* 111:1630–1779
- Orlando S, Miceli M, Pumo ML, Bocchino F. 2015. *ArXiv e-prints*
- Panagia N, Gilmozzi R, Macchetto F, Adorf HM, Kirshner RP. 1991. *Astrophys. J.* 380:L23–L26
- Papaliolios C, Karovska M, Koechlin L, Nisenson P, Standley C, Heathcote S. 1989. *Nature* 338:565
- Pastorello A, Pumo ML, Navasardyan H, Zampieri L, Turatto M, et al. 2012. *Astron. Astrophys.* 537:A141
- Pinto PA, Woosley SE, Ensman LM. 1988. *Astrophys. J.* 331:L101–L104
- Potter TM, Staveley-Smith L, Reville B, Ng CY, Bicknell GV, et al. 2014. *Astrophys. J.* 794:174
- Pun CSJ, Michael E, Zhekov SA, McCray R, Garnavich PM, et al. 2002. *Astrophys. J.* 572:906–931
- Racusin JL, Park S, Zhekov S, Burrows DN, Garmire GP, McCray R. 2009. *Astrophys. J.* 703:1752–1759
- Sana H, de Mink SE, de Koter A, Langer N, Evans CJ, et al. 2013. *Multiplicity of massive O stars and evolutionary implications*. In *370 Years of Astronomy in Utrecht*, eds. G Pugliese, A de Koter, M Wijburg, vol. 470 of *Astronomical Society of the Pacific Conference Series*
- Sapir N, Halbertal D. 2014. *Astrophys. J.* 796:145
- Sapir N, Katz B, Waxman E. 2013. *Astrophys. J.* 774:79
- Sarangi A, Cherchneff I. 2015. *Astron. Astrophys.* 575:A95
- Seitenzahl IR, Taubenberger S, Sim SA. 2009. *Mon. Not. Roy. Astron. Soc.* 400:531–535
- Shivvers I, Zheng W, Silverman J, Modjaz M, Graur O, et al. 2016. In preparation
- Sinnott B, Welch DL, Rest A, Sutherland PG, Bergmann M. 2013. *Astrophys. J.* 767:45
- Smartt SJ, Lennon DJ, Kudritzki RP, Rosales F, Ryans RSI, Wright N. 2002. *Astron. Astrophys.* 391:979–991
- Smith N. 2007. *Astronom. J.* 133:1034–1040
- Smith N, Arnett WD, Bally J, Ginsburg A, Filippenko AV. 2013. *Mon. Not. Roy. Astron. Soc.* 429:1324–1341
- Smith N, Zhekov SA, Heng K, McCray R, Morse JA, Gladders M. 2005. *Astrophys. J.* 635:L41–L44
- Soker N. 1998. *Astrophys. J.* 496:833–841
- Sonneborn G, Fransson C, Lundqvist P, Cassatella A, Gilmozzi R, et al. 1997. *Astrophys. J.* 477:848–864
- Sonneborn G, Pun CSJ, Kimble RA, Gull TR, Lundqvist P, et al. 1998. *Astrophys. J.* 492:L139–L142
- Spyromilio J, Meikle WPS, Allen DA. 1990. *Mon. Not. Roy. Astron. Soc.* 242:669–673
- Staveley-Smith L, Potter TM, Zanzardo G, Gaensler BM, Ng CY. 2014. *Radio Observations of Supernova 1987A*. In *IAU Symposium*, eds. A Ray, RA McCray, vol. 296 of *IAU Symposium*
- Sturm R, Haberl F, Aschenbach B, Hasinger G. 2010. *Astron. Astrophys.* 515:A5
- Sugerman BEK, Crotts APS, Kunkel WE, Heathcote SR, Lawrence SS. 2005. *Astrophys. J. Supp.*

159:60–99

- Taddia F, Sollerman J, Razza A, Gafton E, Pastorello A, et al. 2013. *Astron. Astrophys.* 558:A143
- Taddia F, Stritzinger MD, Sollerman J, Phillips MM, Anderson JP, et al. 2012. *Astron. Astrophys.* 537:A140
- Tanaka T, Washimi H. 2002. *Science* 296:321–322
- Turtle AJ, Campbell-Wilson D, Manchester RN, Staveley-Smith L, Kesteven MJ. 1990. *IAU Circ.* 5086:2
- Tziamtzis A, Lundqvist P, Gröningsson P, Nasoudi-Shoar S. 2011. *Astron. Astrophys.* 527:A35
- Utrobin V, Wongwathanarat A, Janka HT, Mueller E. 2014. *ArXiv e-prints*
- Utrobin VP, Chugai NN. 2005. *Astron. Astrophys.* 441:271–281
- Wang L, Wheeler JC, Höflich P, Khokhlov A, Baade D, et al. 2002. *Astrophys. J.* 579:671–677
- Wesson R, Barlow MJ, Matsuura M, Ercolano B. 2015. *Mon. Not. Roy. Astron. Soc.* 446:2089–2101
- Wongwathanarat A, Müller E, Janka HT. 2015. *Astron. Astrophys.* 577:A48
- Wooden DH, Rank DM, Bregman JD, Witteborn FC, Tielens AGGM, et al. 1993. *Astrophys. J. Supp.* 88:477–507
- Woodsley SE. 1988. *Astrophys. J.* 330:218–253
- Woodsley SE, Hartmann D, Pinto PA. 1989. *Astrophys. J.* 346:395–404
- Xu Y, McCray R. 1991. *Astrophys. J.* 375:190–201
- Zanardo G, Staveley-Smith L, Ball L, Gaensler BM, Kesteven MJ, et al. 2010. *Astrophys. J.* 710:1515–1529
- Zanardo G, Staveley-Smith L, Indebetouw R, Chevalier RA, Matsuura M, et al. 2014. *Astrophys. J.* 796:82
- Zhekov SA, McCray R, Borkowski KJ, Burrows DN, Park S. 2005. *Astrophys. J.* 628:L127–L130
- Zhekov SA, McCray R, Borkowski KJ, Burrows DN, Park S. 2006. *Astrophys. J.* 645:293–302